InstantRetouch: Efficient and High-Fidelity Instruction-Guided Image Retouching with Bilateral Space

Jiarui Wu[1,2], Yujin Wang[1], Ruikang Li[1,2], Fan Zhang[1], Mingde Yao[2], Tianfan Xue[2,1,3]
[1]Shanghai AI Laboratory,[2]CUHK MMLab,[3]CPII under InnoHK
{wj024, tfxue}@ie.cuhk.edu.hk

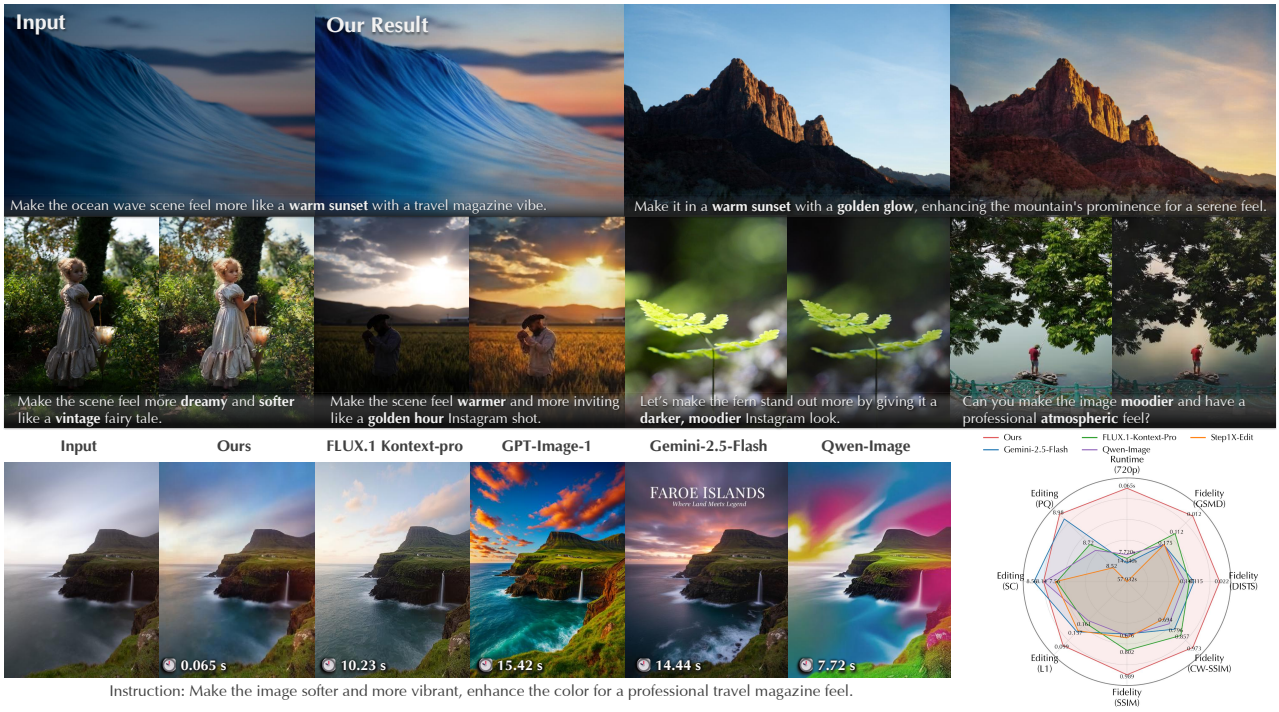

Figure 1. Comparing our method with state-of-the-art image editing methods [6, 22, 28, 43]. As shown in the upper part, our method follows text instructions to generate visually pleasing retouching results while preserving high fidelity, whether for natural landscapes or portraits. In contrast, as demonstrated in the lower section, other state-of-the-art methods modify the original content. Finally, as depicted in the multi-dimensional comparison chart, our method outperforms others in terms of ***fidelity***, ***quality***, and ***speed***.

Abstract

Language-guided photo retouching aims to adjust color and tone while preserving geometry and texture. Recently, diffusion-based retouching shows a superior visual quality, but often struggles with both fidelity issues due to its generative nature and efficiency because of its iterative sampling process. In this work, we propose an efficient and fidelity-preserving retouching method using bilateral space manipulation, which is both compact and content-decoupled. Specifically, instead of directly editing pixels or image latents, our model predicts a low-resolution bilateral grid of affine transforms, which are sliced using a learned guidance map and then applied to the full-resolution image. This approach yields both high fidelity and improved efficiency. To retain strong priors of a pretrained generative model, we distill a multi-step diffusion model into our bilateral grid framework using Variational Score Distillation, complemented by a prompt alignment loss to guide instruction-following behavior. Additionally, we introduce a new benchmark and evaluate our method across multiple dimensions: fidelity, instruction following, and efficiency. Compared to latest editing methods, like Gemini-2.5-Flash (Nano-Banana), our method can avoid content drift, significantly improve latency, and generate visually pleasing

edits, while maintaining a high level of fidelity.

1. Introduction

The ability to automatically retouch photos using natural language instructions represents a significant advancement over traditional image enhancement algorithms [31, 48], which often lack expressive, fine-grained control. This paradigm shift has been driven by large-scale diffusion models [2, 34], capable of producing expressive and visually pleasing results guided by user instructions. Recent work continues to scale up these generative models for general-purpose image editing, as seen in Step-1X-Edit [28], FLUX.1-Kontext [22], Qwen-Image [43], or Gemini-2.5-Flash [6]. These models exhibit a remarkable ability in general-purpose editing, such as adding or removing objects, often producing results that are indistinguishable from real images.

Still, these generative models exhibit limitations in fidelity and efficiency when applied to image retouching. First, for photo retouching, changes must be restricted to photometric adjustments without affecting geometry or texture. Existing generative editing models, however, may not adequately disentangle these edits, leading to unwanted content drift, as shown in Fig. 1. Second, these models, often based on iterative diffusion processes, are computationally expensive and slow, limiting their application for high-resolution image retouching.

These limitations arise because generative editing directly modifies the variational latent of the input image in the diffusion process [34]. The latent representation consists of both actual image content and photometric information (brightness, color, etc.), which is unnecessarily large for retouching, slowing down the process. Manipulating in latent representation may also introduce the risk of changing actual visual content, texture, or geometric structure. Instead, retouch editing should only operate on a smaller representation that only focuses on visual appearance, without content information.

Therefore, we propose to only predict the parameters of a transformation in a compact and content-decoupled *bilateral space*, instead of directly touch original image content. The bilateral manipulation space [4, 5, 12] is instantiated as a low-resolution 3D bilateral grid of affine transforms. A learned guidance map slices this grid to produce per-pixel affine coefficients that are applied to the full-resolution image, enabling complex tonal adjustments. This representation is exceptionally efficient even at 4K resolution and ensures high fidelity by design. As shown in Fig. 1, our solution based on bilateral grids is 70-800 times faster and better preserves fidelity compared with baselines.

While the bilateral space offers an ideal representation for retouching, generating visually pleasing results from instructions still requires the rich semantic priors from diffusion models. However, their slow, iterative inference is fundamentally at odds with our desired efficiency. We resolve this conflict by distilling a multi-step diffusion model into a fast, one-step generator that directly predicts the bilateral grid. In this way, we can leverage the *rich diffusion priors* for visually pleasing results guided by instruction, along with the *fidelity and efficiency* advantages of the bilateral space.

To enable this distillation, we first curate a large-scale, high-quality instruction-retouching dataset to fine-tune a multi-step teacher diffusion model. We then transfer its knowledge to an efficient student network which outputs the bilateral grid in a single forward pass, using a one-step bilateral distillation framework. In this one-step distillation, we employ Variational Score Distillation (VSD) [42, 47] as the core objective, which we augment with a CLIP-based [32] prompt alignment loss. This provides crucial semantic supervision to improve instruction following, particularly for ambiguous or stylistic prompts where pixel-level signals are weak. In addition, we design a bilateral loss to better regularize bilateral grid prediction. At last, we design a progressive distillation strategy to ensure training stability.

To evaluate performance on the instruction-guided retouching task, we introduce a new benchmark, iRetouch, composed of diverse real-world instruction-guided retouching scenarios. We assess models along three key axes: content fidelity, measured by the preservation of original texture and geometry; instruction following, evaluated via text-image alignment metrics and human preference studies; and efficiency, quantified by latency at various resolutions. As demonstrated in Fig. 1, our method is 70-800 times faster than large editing models [2, 6, 17, 22, 28, 43] and achieves superior content fidelity, all while maintaining comparable instruction-following performance.

2. Related Works

Instruction-based Image editing. Image editing enables intuitive image modifications driven by language. Early works, such as InstructPix2Pix [2], fine-tuned diffusion models by creating paired instruction-image datasets. Subsequent research [9, 13, 23, 29, 52] primarily focused on architectural optimizations to improve control granularity and consistency, while others [3, 11, 38, 50] concentrated on data-driven enhancements, expanding the range of instructions and diversifying editing examples. Additionally, some approaches [15, 16, 24, 51] integrated large language model reasoning with diffusion-based image synthesis, while others leveraged chain-of-thought (CoT) reasoning [10] to improve the model's reasoning ability for handling more complex editing tasks. Flow-edit [21] constructs an ordinary differential equation to map the source and target distributions, reducing transport costs in text-driven editing. JarvisArt [26], on the other hand, combines a multi-modal large language model (MLLM)-driven

agent that understands user intent and intelligently coordinates over 200 retouching tools. Recently, image editing has increasingly shifted toward large models with multi-modal fusion [1, 6, 7, 22, 28, 40, 49]. For example, FLUX.1 Kontext [22], as a generative flow matching model, integrates both image generation and editing tasks into a unified architecture, handling both local editing and generative in-context tasks.

Image retouching. Automating the complex task of image style adjustment has seen varied approaches. Early methods like 3D LUTs [31, 48] were fast but confined to fixed styles, while generative models [18] often lack sufficient interpretability and usually alter the original content of the image. More recent works utilized reinforcement learning to automate editing [14, 20, 44]. Tseng *et al*. [39] used neural networks to proxy different image processing modules and optimized the image processing pipeline parameters using a style loss function. However, those methods mentioned above typically handle a single style during training and cannot offer flexible control based on instructions.

3. Method Overview

Our goal is to leverage the *rich diffusion priors* for instruction-guided editing while retaining the *fidelity and efficiency* of the bilateral space. To this end, our method distills a multi-step diffusion model into a fast, one-step generator, G_θ, that directly predicts a bilateral grid. The process unfolds in two main stages. First, we curate a large-scale, high-quality instruction-retouching dataset (Sec. 3.1) to fine-tune a multi-step diffusion teacher, ϵ_ϕ (Sec. 3.2). Second, we distill the knowledge from this teacher into our one-step bilateral grid generator (Sec. 3.3) using a novel distillation framework (Sec. 3.4).

As illustrated in Fig. 2, our generator G_θ consists of two synergistic branches: a low-resolution one-step diffusion branch for semantic understanding and retaining rich diffusion priors, and a full-resolution bilateral processing branch that applies the learned edit to deliver high-fidelity retouching on high-resolution input. However, directly training the proposed bilateral processing network may introduce instability in training; we instead adopt a progressive training strategy. We first train the low-resolution branch by minimizing the Variational Score Distillation loss (Sec. 3.4.1), a data loss (Sec. 3.4.3), and our prompt alignment loss (Sec. 3.4.2). We then jointly optimize both branches, adding a bilateral loss (Sec. 3.4.4) to optimize the full-res bilateral branch.

3.1. Training Dataset

Training diffusion models relies on large-scale data. Existing instruction-editing datasets primarily focus on object-level or geometric edits and lack the fine-grained, high-fidelity examples needed for photo retouching. We therefore construct a new dataset of $\sim$ 200K triplets $(x, x^\star, c_T)$, where x is the input image, $x^\star$ is a high-quality retouched target, and c_T is a textual instruction. Our dataset is built via a controlled degradation process.

High-quality targets. We curate visually pleasing images from public datasets and the web, filtered by no-reference image quality metrics MUSIQ [19] and LAION aesthetic score [37] with conservative thresholds, yielding targets $x^\star$.

Input image generation. For each target $x^\star$, we synthesize a degraded input x by applying random photometric adjustments via a photo-finishing pipeline [44]. This includes perturbations to exposure, gamma, white balance, contrast, tone curves, saturation, shadows/highlights, and HSL. To simulate local retouching, we generate region masks using a Grounding-SAM procedure [27, 33] and additional soft masks from simple priors, applying different degradation parameters within each mask to induce spatially varying edits while preserving fidelity.

Instruction generation. Given $(x, x^\star)$, we prompt a multi-modal LLM (Qwen2.5-VL-72B [1]) in a role-playing template to generate concise, diverse photo-finishing instructions c_T that describe the transformation from x to $x^\star$. A small rule-based checker enforces diversity and filters content-edit verbs. Further details on dataset construction are in the Appendix.

3.2. Pretrained Multi-step Diffusion

Following InstructPix2Pix [2], our teacher model ϵ_ϕ is a UNet trained to predict the noise added to a target image's latent representation. Let x be the input image, $x^\star$ the target, and c_T the text instruction. We operate in the VAE latent space of a pre-trained Stable Diffusion model [34], with encoder $\mathcal{E}_\phi$ and decoder $\mathcal{D}_\phi$. During training, noise ϵ is added to the target latent $z_0 = \mathcal{E}_\phi(x^\star)$ to create a noisy latent $z_t = \alpha_t z_0 + \beta_t \epsilon$. The teacher ϵ_ϕ is trained with an MSE loss to predict this noise, conditioned on the input image latent $c_I = \mathcal{E}_\phi(x)$ and the text prompt c_T:

$$\mathcal{L}_{\text{teacher}}(\phi) = \mathbb{E}_{x,x^\star,c_T,t,\epsilon}\Big[\big\|\epsilon - \epsilon_\phi\big(z_t,\ t,\ c_I,\ c_T\big)\big\|_2^2\Big]. \tag{1}$$

However, applying this multi-step diffusion model for retouching is slow and prone to content drift. We therefore distill from this heavy pretrained editor into a lightweight, one-step retouching model designed to guarantee content fidelity, discussed below.

3.3. One-step Bilateral Generator

As shown in Fig. 2, our lightweight one-step bilateral grid generator is composed of two branches: a low-resolution diffusion branch and a full-resolution bilateral processing branch. The low-resolution branch contains a frozen VAE encoder $\mathcal{E}_\theta$ and a one-step U-Net denoiser ϵ_θ, tasked with semantic understanding and preserving the rich diffusion priors. During training, a VAE decoder is temporarily employed to generate a low-resolution image, which helps to stabilize the distillation process.

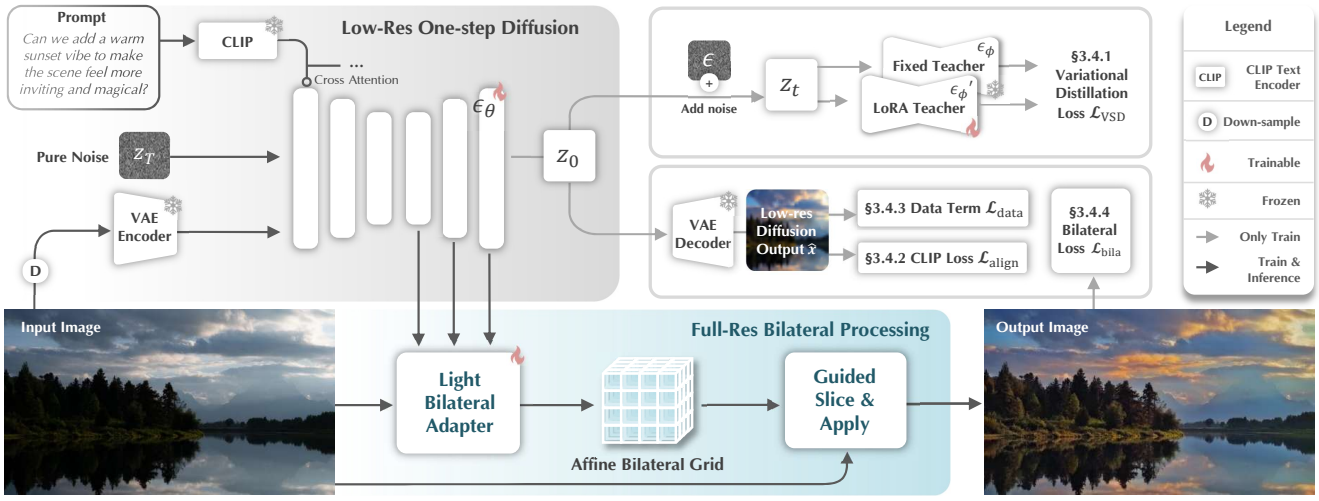

Figure 2. Our framework distills a multi-step diffusion teacher into a fast, one-step generator composed of two synergistic branches. The low-resolution diffusion branch processes the input image and text instruction to understand the edit, and then uses a light bilateral adapter to predict the parameters of a bilateral grid. The full-resolution branch then applies this grid to the original high-res image, producing the final high-fidelity result. We use Variational Score Distillation (VSD) to transfer the teacher's knowledge and a CLIP-based language alignment loss to ensure instruction alignment.

The full-resolution branch contains a lightweight bilateral adapter. In a single forward step, it generates a bilateral grid [4] $\Gamma \in \mathbb{R}^{H_g \times W_g \times D \times 12}$ that stores local affine transformation parameters in 3D space. This grid is then processed by a fully differentiable "slice-and-apply" operator that acts on the full-resolution input image of size (H, W). For each input pixel with coordinates (x', y') and color (r, g, b), the operator first computes a grayscale guidance value $z = g(r, g, b)$ via a learned lookup table. It then uses the pixel's spatial coordinates and this guidance value to retrieve a specific affine matrix A by slicing the grid with trilinear interpolation: $A = \Gamma(x' W_g/W, y' H_g/H, z/d)$. Finally, this matrix is applied to the original pixel color, $O = A \cdot (r, g, b, 1)^T$, to produce the final output. This entire mechanism delivers efficient and high-fidelity retouching directly on the high-resolution image.

Our model is highly efficient due to its design. The full-resolution operators have negligible runtime, even at 4K resolution. And the low-resolution branch has constant latency at different resolutions. This enables 4K image processing in just 68ms, vastly outperforming diffusion methods requiring over 10s for 720p inputs.

3.4. One-step Bilateral Distillation

Although the proposed one-step generator G_θ is super-efficient and guarantees no content drift by design, it has a very different structure compared with the pretrained teacher network ϵ_ϕ (diffusion model), posing a challenge in distillation. Therefore, we proposed a novel progressive distillation strategy, described below.

3.4.1. Variational Score Distillation in Latent Space

In the low-res one-step diffusion branch, the frozen VAE encoder and decoder are initialized from the weights of pretrained VAE $\mathcal{E}_\phi$ and $\mathcal{D}_\phi$, and the denoising network ϵ_θ is initialized from the weights of pretrained denoiser ϵ_ϕ. Recall that diffusion models utilize a UNet to predict the noise $\hat{\epsilon}$ in noisy latent z_t, and the denoised latent can be obtained as $\hat{z}_0 = \frac{z_t - \beta_t \hat{\epsilon}}{\alpha_t}$. We directly conducting one-step denoising on the white noise $z_{t_{max}} \sim \mathcal{N}(0, I)$, conditioned on $c_I = \mathcal{E}_\theta(x)$ and c_T, to predict the clean latent $\hat{z}_0$ is calculated as:

$$\hat{z}_0 = \frac{z_{t_{max}} - \beta_t \epsilon_\theta(z_{t_{max}},\ t_{max},\ c_I,\ c_T)}{\alpha_t}, \tag{2}$$

and the corresponding low-resolution image is $\hat{x} = \mathcal{D}_\theta(\hat{z}_0)$. Note that during inference, the VAE decoder is not used, as $\hat{x}$ only helps to stabilize the distillation process, and is not needed in full-res bilateral processing. We regularize ϵ_θ with a latent-space Variational Score Distillation (VSD) loss, $\mathcal{L}_{\text{VSD}}$, following the design in DMD [47].

VSD loss introduces a trainable regularizer $\epsilon_{\phi'}$ finetuned on the distribution of generated images $\hat{x}$ of the one-step generator ϵ_θ to replicate its behaviour. Given the clean latent predicted by the one-step generator via Eqn. 2, we add noise to it to construct the noisy latent $\hat{z}_t = \alpha_t \hat{z}_0 + \beta_t \epsilon$. This $\hat{z}_t$ then serves as a common input to the teacher and regularizer to compute a stable gradient that steers the student towards the teacher. We adopt the latent form of VSD used in DMD [45, 47]. The gradient of the VSD loss w.r.t. θ $\nabla_\theta \mathcal{L}_{\text{VSD}}$ is

$$\mathbb{E}_{t,\epsilon,\hat{z}_t}\Big[\omega(t)\big(\epsilon_\phi(\hat{z}_t, t, c_I, c_T) - \epsilon_{\phi'}(\hat{z}_t, t, c_I, c_T)\big)\frac{\partial \hat{z}_0}{\partial \theta}\Big], \tag{3}$$

To ensure the regularizer $\epsilon_{\phi'}$ remains a faithful proxy for the generator's current state, it is trained concurrently on noisy samples $\hat{z}_t$ derived from the generator's own outputs $\hat{z}_0$:

$$\mathcal{L}_{\text{diff}}(\phi') = \mathbb{E}_{t,\epsilon,c_I,c_T,\hat{z}_t}\left[\|\epsilon_{\phi'}(\hat{z}_t, t, c_I, c_T) - \epsilon\|_2^2\right]. \quad (4)$$

To further stabilize this process, we adopt a progressive schedule. Training begins with high noise levels ($t \in [t_{\text{hi}}, t_{max}]$) to learn coarse attributes like tone and exposure, before we gradually lower t_{hi} to distill fine-grained color details.

3.4.2. Prompt Alignment Loss

Distilling a multi-step editor into one step often weaken the coupling between the instruction c_T and often yields "plausible but misdirected" retouches under weak, aesthetic instructions. Thus, we need to add further supervision to ensure the output image follows the users' instructions.

Specifically, unlike object edits, retouching intents are mostly *directional and compositional* (e.g., warmer, dreamy, cinematic). While the VSD loss and data loss ensure feasibility, they do not guarantee that the change follows the intended semantic direction. We therefore convert user instruction c_T into a small set of atomic *retouching attributes* $\mathcal{A}(c_T) = \{a\}$ using a rule-based matcher. Each attribute is an explicit edit direction tailored to photo retouching (e.g., `brightness:up`, `contrast:down`, `mood:cozy`, `temperature:warm`, `style:vintage`) and is paired with two short text prompts describing positive and negative directions. (e.g., "Bright Image" vs. "Dark Image"). This *attribute bank* turns a long, weak instruction into several stable, additive supervision signals. Let $\mathbf{e}^{\text{img}}(\cdot)$ and $\mathbf{e}^{\text{text}}(\cdot)$ be frozen CLIP image and text encoders. The cosine similarity of the two ℓ_2-normalized image and text embeddings is used and its scalar value is denoted by s. For an attribute a (e.g., `mood:cozy`) with prompts (p_a^+, p_a^-) , define $s_a^+ = \langle \mathbf{e}^{\text{img}}(\hat{x}), \mathbf{e}^{\text{text}}(p_a^+)\rangle$ and $s_a^- = \langle \mathbf{e}^{\text{img}}(\hat{x}), \mathbf{e}^{\text{text}}(p_a^-)\rangle$, where $\langle\cdot,\cdot\rangle$ denotes cosine similarity. The per-attribute InfoNCE loss [30] (viewed as a function of a) is

$$\ell_{\text{nce}}(a) = -\log \frac{\exp(s_a^+/\tau)}{\exp(s_a^+/\tau) + \exp(s_a^-/\tau)}. \quad (5)$$

Finally, with confidences w_a from the matcher, the language alignment loss is applied to the one-step branch during distillation:

$$\mathcal{L}_{\text{align}} = \frac{1}{|\mathcal{A}(c_T)|} \sum_{a \in \mathcal{A}(c_T)} \Big[w_a \, \ell_{\text{nce}}(a) \Big]. \quad (6)$$

This supervision restores directional alignment lost by step compression, and resolves ambiguity among many color transforms that could otherwise minimize the data term and VSD term yet deviate from c_T.

3.4.3. Data Supervision Loss

To stabilize distillation, we also add a data term that supervises the low-resolution output $\hat{x}$ with the ground truth target $x^\star$, following [45, 47]:

$$\mathcal{L}_{\text{data}} = \|\hat{x} - x^\star\|_2^2 + \lambda_{\text{LPIPS}} \mathcal{L}_{\text{LPIPS}}(\hat{x}, x^\star). \quad (7)$$

3.4.4. Bilateral Loss

The losses above focus on training the low-resolution branch. To also train the full-resolution bilateral processing branch, we introduce $\mathcal{L}_{\text{bila}}$. Let $\hat{x}_B$ be the final high-resolution output. This loss includes: (i) ℓ_1 and LPIPS losses against the ground truth $x^\star$, (ii) a perceptual agreement term encouraging $\hat{x}_B$ to match the low-res prediction $\hat{x}$, and (iii) a laplacian regularizers on the bilateral grid Γ for smoothness and a penalty that prevents RGB overflow:

$$\begin{aligned}\mathcal{L}_{\text{bila}} = \lambda_1 \| \hat{x}_B - x^\star \|_1 + \lambda_2 \cdot \mathcal{L}_{\text{LPIPS}}(\hat{x}_B, x^\star) \\ + \lambda_3 \cdot \mathcal{L}_{\text{LPIPS}}\big(\hat{x}_B, \hat{x}\big) \\ + \lambda_4 \cdot \|\Delta^3 \Gamma\|_2^2 + \lambda_5 \cdot \Psi(\hat{x}_B), \end{aligned} \quad (8)$$

where Δ^3 is a 3D Laplacian regularizer to penalize differences between adjacent cells over the bilateral grid for smoothness, and Ψ is a soft penalty discouraging out-of-gamut RGB.

3.4.5. Overall Objective and Distillation Strategy

Combining all training losses above, we finally design a novel two-stage progressive distillation strategy.

Stage 1: Low-Resolution one-step diffusion branch training. In this stage, we only train the low-resolution one-step diffusion branch. Note that the low-resolution branch shares the same network structure as the pretrained diffusion and thus distillation training is easier compared with the bilateral processing network. During training, we optimize the U-Net ϵ_θ and the VSD regularizer $\epsilon_{\phi'}$. The objective combines VSD, the data term, and our prompt alignment loss:

$$\mathcal{L}_{\text{stage1}} = \mathcal{L}_{\text{data}} + \lambda_{\text{VSD}} \mathcal{L}_{\text{VSD}} + \lambda_{\text{align}} \mathcal{L}_{\text{align}}. \quad (9)$$

Stage 2: Joint bilateral distillation. After the first stage converges, we unfreeze the bilateral adapter and train the entire generator end-to-end. Since stage 1 already trains the relative heavy low-resolution network, finetuning the lightweight full-resolution bilateral processing is also trackable. To train the bilateral processing, a bilateral loss is added:

$$\mathcal{L}_{\text{stage2}} = \mathcal{L}_{\text{stage1}} + \lambda_{\text{bila}} \mathcal{L}_{\text{bila}}. \quad (10)$$

This complete *one-step bilateral distillation* framework yields an efficient model that guarantees high-fidelity, content-preserving retouching while retaining strong instruction-following capabilities.

4. Experiments

4.1. Experiment Setup

New benchmark iRetouch. For evaluation, we have created a new benchmark, iRetouch, consisting of 500 real-world before-and-after retouching pairs from the Adobe Lightroom community. Instructions for these pairs are generated using our method from Sec. 3.1, followed by manual refinement for clarity and diversity. The benchmark spans a wide variety of scenes (e.g., portraits, landscapes) and includes a rich vocabulary of retouching edits, such as global

Table 1. Comparison on iRetouch benchmark. Our method achieves state-of-the-art efficiency and content fidelity while remaining highly competitive in editing quality. Blank entries indicate models that cannot process high resolutions or are not instruction-driven.

Method	Runtime(s)				Content Fidelity				Editing Quality				
	720p↓	1K↓	2K↓	4K↓	SSIM↑	CW-SSIM↑	GSMD↓	DISTS↓	L1↓	L2↓	SC↑	PQ↑	O↑
3DLUT [48]	0.066	0.079	0.112	0.201	0.982	**0.981**	0.013	0.024	0.136	0.034	-	-	-
RSFNet [31]	**0.029**	**0.047**	0.086	0.189	0.975	0.976	**0.012**	0.038	0.137	0.034	-	-	-
InstructPix2Pix [2]	4.632	-	-	-	0.742	0.768	0.149	0.177	0.164	0.050	7.11	7.58	7.34
Step1X-Edit [28]	57.932	-	-	-	0.706	0.694	0.174	0.167	0.140	0.036	7.63	8.52	8.06
GPT-Image-1 [17]	15.427	21.889	-	-	0.505	0.397	0.242	0.216	0.215	0.082	8.09	8.56	8.32
Qwen-Image [43]	7.720	-	-	-	0.689	0.744	0.174	0.147	0.168	0.054	8.12	8.67	8.39
FLUX.1-Kontext-Pro [22]	10.235	-	-	-	0.802	0.857	0.112	0.132	0.161	0.050	7.56	8.72	8.12
Gemini-2.5-Flash [6]	14.440	-	-	-	0.676	0.796	0.175	0.115	0.137	0.036	**8.56**	8.94	**8.74**
Ours	0.065	0.065	**0.066**	**0.068**	**0.989**	0.973	**0.012**	**0.022**	**0.099**	**0.018**	8.14	**8.98**	8.54

adjustments, specific styles (cinematic, dreamy), moods, and local effects (see Appendix for a detailed breakdown).

Content fidelity metrics. Retouching is non-destructive, so edits must preserve structure and texture without repaints. To factor out intentional tone changes, we convert outputs to grayscale and histogram-match them to the input, then compute SSIM [41] (structural similarity), CW-SSIM [35] (geometry and texture distortion), DISTS [8] (textural similarity), and GMSD [46] (gradient-magnitude consistency).

Editing quality metrics. Following prior work [28, 50], we report L1/L2 distances, instruction–image alignment (SC, 0–10), perceptual quality (PQ, 0–10), and the overall score $\mathrm{O} = \sqrt{\mathrm{SC} \times \mathrm{PQ}}$. SC and PQ are generated using GPT-4o, similar to [28]. Additional details are provided in the Appendix.

Implementation. Our one-step bilateral generator is built upon a pre-trained Stable Diffusion editor. We initialize our student U-Net from the teacher's weights and freeze the VAE. VSD distillation follows a three-stage curriculum over timesteps to learn from coarse structure and tone (high t), then instruction alignment (mid t), and finally fine-grained color details (low t). Training is at 512px using AdamW with EMA, mixed precision, and gradient clipping. Inference is a single pass: the model generates a bilateral grid and applies it to the native resolution input, yielding constant-time performance regardless of image size. We train on our instruction-retouching dataset in Sec. 3.1. See the Appendix for full implementation details.

Runtime. We measure end-to-end latency across resolutions from 720p to 4K. Open-source models are benchmarked on a server with 8 NVIDIA RTX 4090 GPUs. For proprietary models, we report the full end-to-end API latency, including data transfer.

4.2. Evaluation and Results

We compare our method with baselines across three categories: (1) traditional enhancement methods [31, 48], (2) open-source image editing models [2, 28, 43], and (3) proprietary large-scale editing models [6, 17, 22].

4.2.1. Evaluation on Our iRetouch Benchmark

As shown in Tab. 1, our method outperforms others in terms of runtime, fidelity, and editing quality.

Efficiency. Our model demonstrates exceptional efficiency, maintaining a near-constant inference time of 0.065–0.068s from 720p up to 4K resolutions. This represents a 70–900× speedup over generative baselines at 720p. The blank runtime entries for some baselines highlight a critical limitation: most diffusion-based models cannot natively process resolutions beyond 1K, a barrier our design overcomes.

Fidelity. Our approach achieves state-of-the-art content fidelity among all instruction-guided models. This confirms our bilateral branch successfully prevents the textural distortions common in pure diffusion editors.

Quality. For editing quality, our model's overall score (O) of 8.54 is highly competitive with the top proprietary system (Gemini-2.5-Flash at 8.74) and significantly surpasses other open-source editors. The blank quality scores for traditional methods like 3D LUT exist because they are not instruction-driven and thus cannot be evaluated for semantic alignment. In summary, our method delivers near–state-of-the-art editing quality with state-of-the-art fidelity and 4K-constant runtime. These results support our design goal: instruction-guided retouching that is high-fidelity, fast, and stable across resolutions. We also provide a more detailed analysis of the relationship between quality and fidelity in the Appendix.

Visual comparison. Fig. 3 provides a qualitative comparison across a range of instructions. The results highlight a common failure in competing methods: a trade-off between editing quality and content fidelity. Generative editors like InstructPix2Pix and GPT-Image-1 often introduce severe artifacts, hallucinations, or unwanted text overlays, fundamentally altering the source image. Even capable models like Gemini-2.5-Flash can subtly change key features. Our method, however, successfully follows both global and local instructions while maintaining high fidelity, applying the desired stylistic edits without distorting content or compromising the original photograph's integrity.

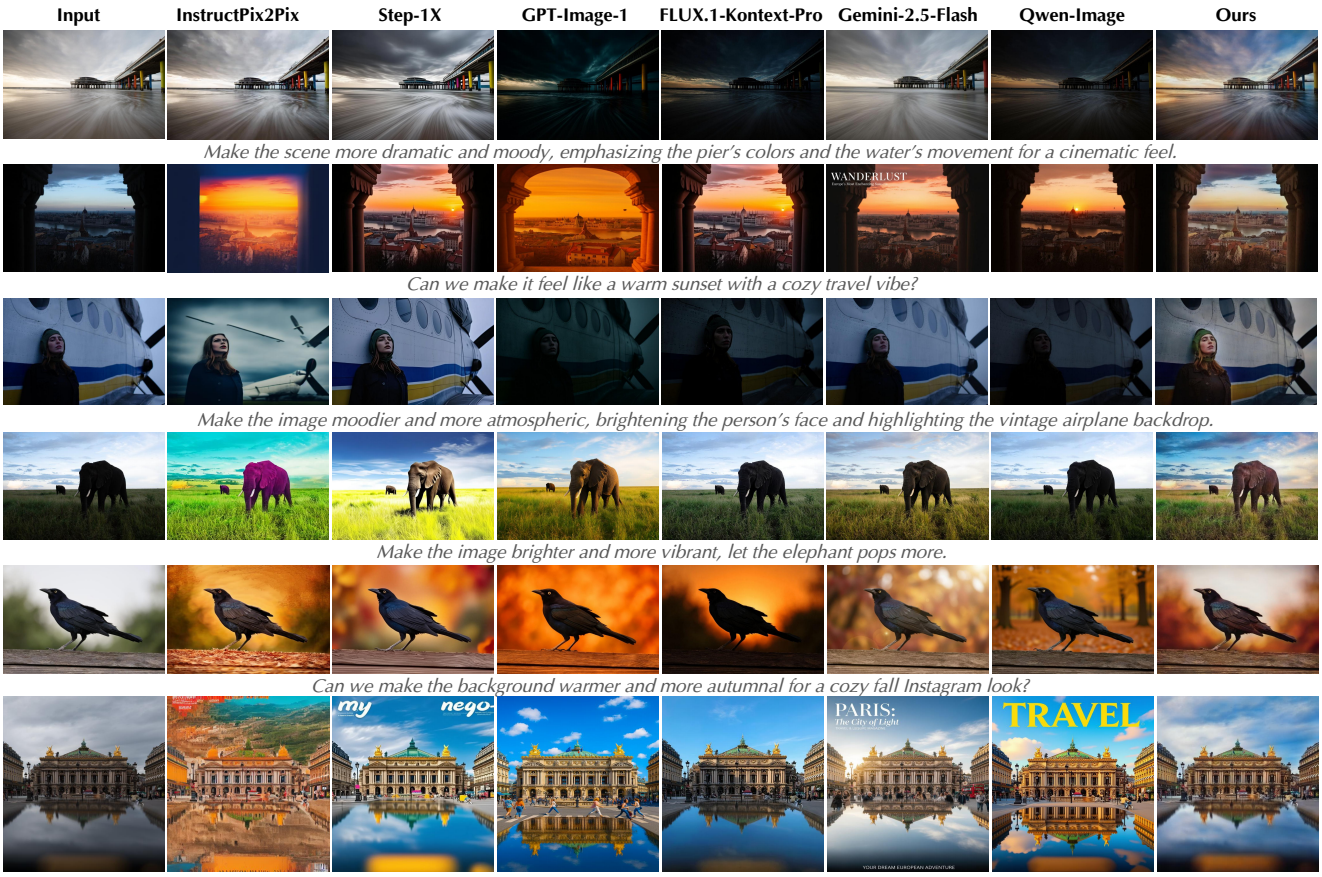

Figure 3. Visual comparisons of different image editing methods on our iRetouch benchmark.

4.2.2. User Study

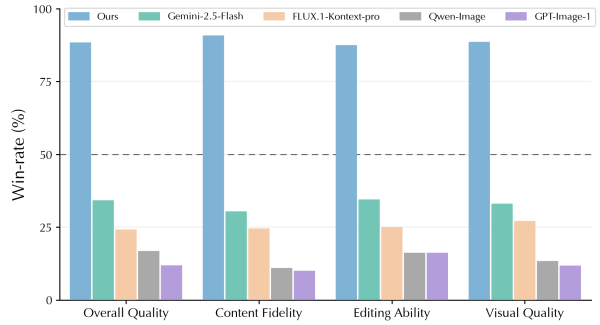

Figure 4. User preference study results on iRetouch benchmark.

To assess subjective user preference, we conducted a user study with 30 participants, who evaluated 20 retouching examples from our iRetouch benchmark. They compared our method against four leading baselines (FLUX.1-Kontext-pro, Gemini-2.5-Flash, Qwen-Image, GPT-Image-1) across four dimensions: content fidelity, editing ability, visual quality, and overall preference. As shown in Fig. 4, the results reveal a clear and consistent preference for our method. Our approach achieved the highest ratings in all categories, confirming that users favor its artifact-free, high-fidelity edits that accurately reflect their intent.

4.2.3. Evaluation of Identity Preservation on PPR10K

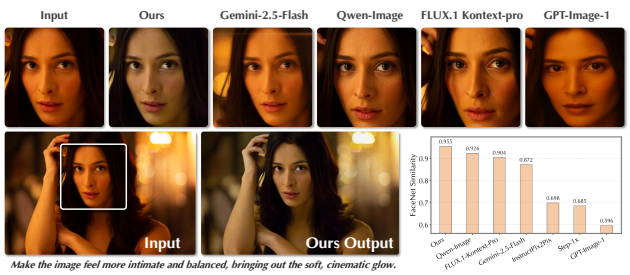

Figure 5. Results of identity preservation comparison on the PPR10K dataset. Our model scores highest in facial similarity and avoids the identity-altering artifacts.

In portrait editing, content fidelity is crucial as it requires strict identity preservation. To evaluate identity preservation on this task, we test on 100 images from the PPR10K dataset [25] with MLLM generated instructions. We quantify identity preservation by extracting facial embeddings from the input and output images using FaceNet [36] and then computing their cosine similarity. As shown quantitatively in Fig. 5, our method achieves the highest face similarity score. We also include qualitative comparison in the figure; our model retouches the portrait while strictly preserving fidelity, whereas competing methods introduce no-

Figure 6. Visualization of ablation study on the loss configuration of one-step bilateral distillation.

ticeable repainting that distorts the subject's identity.

4.3. Ablation

We conduct a series of ablation studies to validate our key design choices, focusing on our framework and the components of our distillation algorithms.

Table 2. Ablation study on our framework. We evaluate content fidelity, editing quality, and runtime. Our full model effectively combines the strengths of diffusion priors and bilateral processing, achieving high scores across all criteria.

Method	Runtime(s)↓	Content Fidelity			Editing Quality		
		SSIM↑	GSMD↓	DISTS↓	SC↑	PQ↑	O↑
Bilateral Grid Prediction	0.001	0.996	0.003	0.005	4.48	8.28	6.09
Teacher (Multi-step Diffusion)	4.602	0.833	0.095	0.121	7.96	8.71	8.33
Hybrid (Teacher Features + Bilateral)	0.065	0.904	0.073	0.107	5.65	7.62	6.56
Student (Diffusion-Only)	0.319	0.788	0.130	0.152	8.43	8.85	8.64
Ours (Full Model)	**0.065**	**0.989**	**0.012**	**0.022**	**8.14**	**8.98**	**8.54**

Ablation on framework. We first analyze the contribution of our framework components in Tab. 2. We compare our full model against four key baselines: (1) *Bilateral Grid Prediction*, a model that directly predicts a bilateral grid from the input image without diffusion priors, trained on our dataset; (2) our *Teacher (Multi-step Diffusion)* model; (3) a *Hybrid* model that uses features from the multi-step teacher to predict a bilateral grid; and (4) our *Student (Diffusion-Only)*, which corresponds to the low-resolution RGB output from our distilled U-Net without the bilateral branch.

The results in Tab. 2 reveal a clear trade-off. Purely diffusion-based models (Teacher, Student-Only) achieve high editing quality but low fidelity. In contrast, a simple Bilateral Grid Prediction model preserves content perfectly (0.996 SSIM) but fails to follow instructions (6.09 O-score). Our full model uniquely resolves this conflict by merging the semantic strength of diffusion (8.54 O-score) with the structural preservation of bilateral processing (0.989 SSIM), all while maintaining high efficiency. This validates our dual-branch design for balancing fidelity, quality, and speed.

Ablation on one-step bilateral distillation. Next, we validate the effectiveness of the core loss components in our one-step bilateral distillation process. As shown in Tab. 3, we start with a base objective, $\mathcal{L}_{\text{base}}$, which includes only the data term and bilateral losses ($\mathcal{L}_{\text{data}} + \mathcal{L}_{\text{bila}}$). We then progressively add our main distillation loss, $\mathcal{L}_{\text{VSD}}$, and our prompt alignment loss, $\mathcal{L}_{\text{align}}$.

Table 3. Ablation on our distillation loss components. Both VSD and our prompt alignment loss ($\mathcal{L}_{\text{align}}$) are critical for achieving high editing quality.

Loss Configuration	Editing Quality		
	SC↑	PQ↑	O↑
$\mathcal{L}_{\text{base}}$	5.978	8.280	7.036
$\mathcal{L}_{\text{base}} + \mathcal{L}_{\text{VSD}}$	7.257	9.013	8.087
$\mathcal{L}_{\text{base}} + \mathcal{L}_{\text{VSD}} + \mathcal{L}_{\text{align}}$	8.14	8.984	8.553

As shown in Tab. 3, the base model ($\mathcal{L}_{\text{base}}$) alone is insufficient for quality editing. Adding $\mathcal{L}_{\text{VSD}}$ is critical, dramatically boosting the score by transferring the teacher's generative priors. Incorporating our prompt alignment loss ($\mathcal{L}_{\text{align}}$) provides a final, significant gain. This confirms its role in providing essential directional supervision for interpreting stylistic prompts where VSD alone falls short. We also visualize this ablation in Fig. 6.

4.4. Fine-grained Control

Figure 7. Visualization of continuous control on editing strength.

Our framework's control extends beyond language prompts to include more fine-grained control over the retouching effect. As shown in Fig. 7, users can continuously adjust the retouching intensity by applying a scalar s to the per-pixel affine transforms. Thanks to the linearity of the affine transform in bilateral space, setting $s = 0$ yields the input, while $s > 1$ enhances the effect. This transforms our model into a smart, language-guided filter, offering precise control where language can be ambiguous. Moreover, we support fine-grained regional control using a soft bilateral blending strategy, which is further detailed in the Appendix.

5. Conclusion

In this work, we present an efficient and fidelity-preserving approach to image retouching that addresses both fidelity degradation and computational inefficiency. Instead of manipulating pixels or latent features, our method operates in a compact, content-decoupled bilateral space, enabling high fidelity with significantly improved efficiency. To preserve strong generative priors, we distill a multi-step diffusion model into our bilateral grid framework via variational score distillation, enhanced with a CLIP-based contrastive loss for instruction following. We further introduce a new benchmark dataset for instruction-guided

retouching and evaluate fidelity, instruction alignment, and efficiency. Compared to recent image editing methods such as Gemini-2.5-Flash (Nano Banana), our approach runs orders of magnitude faster while achieving superior content fidelity and comparable instruction-following performance.

References

[1] Shuai Bai, Keqin Chen, Xuejing Liu, Jialin Wang, Wenbin Ge, Sibo Song, Kai Dang, Peng Wang, Shijie Wang, Jun Tang, et al. Qwen2. 5-vl technical report. *arXiv preprint arXiv:2502.13923*, 2025. 3, 2

[2] Tim Brooks, Aleksander Holynski, and Alexei A Efros. Instructpix2pix: Learning to follow image editing instructions. In *Proceedings of the IEEE/CVF Conference on Computer Vision and Pattern Recognition*, pages 18392–18402, 2023. 2, 3, 6, 5, 9

[3] Tuhin Chakrabarty, Kanishk Singh, Arkadiy Saakyan, and Smaranda Muresan. Learning to follow object-centric image editing instructions faithfully. In *Findings of the Association for Computational Linguistics: EMNLP 2023*, pages 9630–9646, Singapore, 2023. Association for Computational Linguistics. 2

[4] Jiawen Chen, Sylvain Paris, and Frédo Durand. Real-time edge-aware image processing with the bilateral grid. *ACM Transactions on Graphics (TOG)*, 26(3):103–es, 2007. 2, 4

[5] Jiawen Chen, Andrew Adams, Neal Wadhwa, and Samuel W Hasinoff. Bilateral guided upsampling. *ACM Transactions on Graphics (TOG)*, 35(6):1–8, 2016. 2, 7

[6] Gheorghe Comanici, Eric Bieber, Mike Schaekermann, Ice Pasupat, Noveen Sachdeva, Inderjit Dhillon, Marcel Blistein, Ori Ram, Dan Zhang, Evan Rosen, et al. Gemini 2.5: Pushing the frontier with advanced reasoning, multimodality, long context, and next generation agentic capabilities. *arXiv preprint arXiv:2507.06261*, 2025. 1, 2, 3, 6, 5

[7] Chaorui Deng, Deyao Zhu, Kunchang Li, Chenhui Gou, Feng Li, Zeyu Wang, Shu Zhong, Weihao Yu, Xiaonan Nie, Ziang Song, et al. Emerging properties in unified multimodal pretraining. *arXiv preprint arXiv:2505.14683*, 2025. 3

[8] Keyan Ding, Kede Ma, Shiqi Wang, and Eero P Simoncelli. Image quality assessment: Unifying structure and texture similarity. *IEEE transactions on pattern analysis and machine intelligence*, 44(5):2567–2581, 2020. 6, 9

[9] Zheng-Peng Duan, Jiawei Zhang, Zheng Lin, Xin Jin, Xun-Dong Wang, Dongqing Zou, Chun-Le Guo, and Chongyi Li. Diffretouch: Using diffusion to retouch on the shoulder of experts. In *Proceedings of the AAAI Conference on Artificial Intelligence*, pages 2825–2833, 2025. 2, 4, 5

[10] Tsu-Jui Fu, Wenze Hu, Xianzhi Du, William Yang Wang, Yinfei Yang, and Zhe Gan. Guiding instruction-based image editing via multimodal large language models. *arXiv preprint arXiv:2309.17102*, 2023. 2

[11] Zigang Geng, Binxin Yang, Tiankai Hang, Chen Li, Shuyang Gu, Ting Zhang, Jianmin Bao, Zheng Zhang, Houqiang Li, Han Hu, et al. Instructdiffusion: A generalist modeling interface for vision tasks. In *Proceedings of the IEEE/CVF Conference on computer vision and pattern recognition*, pages 12709–12720, 2024. 2

[12] Michaël Gharbi, Jiawen Chen, Jonathan T Barron, Samuel W Hasinoff, and Frédo Durand. Deep bilateral learning for real-time image enhancement. *ACM Transactions on Graphics (TOG)*, 36(4):1–12, 2017. 2, 7

[13] Qin Guo and Tianwei Lin. Focus on your instruction: Fine-grained and multi-instruction image editing by attention modulation. In *Proceedings of the IEEE/CVF Conference on Computer Vision and Pattern Recognition*, pages 6986–6996, 2024. 2

[14] Yuanming Hu, Hao He, Chenxi Xu, Baoyuan Wang, and Stephen Lin. Exposure: A white-box photo post-processing framework. *ACM Transactions on Graphics (TOG)*, 37(2): 1–17, 2018. 3

[15] Yujia Hu, Songhua Liu, Zhenxiong Tan, Xingyi Yang, and Xinchao Wang. Image editing as programs with diffusion models. *arXiv preprint arXiv:2506.04158*, 2025. 2

[16] Yuzhou Huang, Liangbin Xie, Xintao Wang, Ziyang Yuan, Xiaodong Cun, Yixiao Ge, Jiantao Zhou, Chao Dong, Rui Huang, Ruimao Zhang, et al. Smartedit: Exploring complex instruction-based image editing with multimodal large language models. In *Proceedings of the IEEE/CVF Conference on Computer Vision and Pattern Recognition*, pages 8362–8371, 2024. 2

[17] Aaron Hurst, Adam Lerer, Adam P Goucher, Adam Perelman, Aditya Ramesh, Aidan Clark, AJ Ostrow, Akila Welihinda, Alan Hayes, Alec Radford, et al. Gpt-4o system card. *arXiv preprint arXiv:2410.21276*, 2024. 2, 6, 5

[18] Tero Karras, Samuli Laine, and Timo Aila. A style-based generator architecture for generative adversarial networks. In *Proceedings of the IEEE/CVF conference on computer vision and pattern recognition*, pages 4401–4410, 2019. 3

[19] Junjie Ke, Qifei Wang, Yilin Wang, Peyman Milanfar, and Feng Yang. Musiq: Multi-scale image quality transformer. In *Proceedings of the IEEE/CVF international conference on computer vision*, pages 5148–5157, 2021. 3, 4

[20] Satoshi Kosugi and Toshihiko Yamasaki. Unpaired image enhancement featuring reinforcement-learning-controlled image editing software. In *Proceedings of the AAAI conference on artificial intelligence*, pages 11296–11303, 2020. 3

[21] Vladimir Kulikov, Matan Kleiner, Inbar Huberman-Spiegelglas, and Tomer Michaeli. Flowedit: Inversion-free text-based editing using pre-trained flow models. In *Proceedings of the IEEE/CVF International Conference on Computer Vision*, pages 19721–19730, 2025. 2

[22] Black Forest Labs, Stephen Batifol, Andreas Blattmann, Frederic Boesel, Saksham Consul, Cyril Diagne, Tim Dockhorn, Jack English, Zion English, Patrick Esser, et al. Flux. 1 kontext: Flow matching for in-context image generation and editing in latent space. *arXiv preprint arXiv:2506.15742*, 2025. 1, 2, 3, 6, 5

[23] Sijia Li, Chen Chen, and Haonan Lu. Moecontroller: Instruction-based arbitrary image manipulation with mixture-of-expert controllers. *arXiv preprint arXiv:2309.04372*, 2023. 2

[24] Shufan Li, Harkanwar Singh, and Aditya Grover. Instructany2pix: Flexible visual editing via multimodal instruction following. *arXiv preprint arXiv:2312.06738*, 2023. 2

[25] Jie Liang, Hui Zeng, Miaomiao Cui, Xuansong Xie, and Lei Zhang. Ppr10k: A large-scale portrait photo retouching dataset with human-region mask and group-level consistency. In *Proceedings of the IEEE/CVF Conference on Computer Vision and Pattern Recognition*, pages 653–661, 2021. 7

[26] Yunlong Lin, Zixu Lin, Kunjie Lin, Jinbin Bai, Panwang Pan, Chenxin Li, Haoyu Chen, Zhongdao Wang, Xinghao Ding, Wenbo Li, et al. Jarvisart: Liberating human artistic creativity via an intelligent photo retouching agent. *arXiv preprint arXiv:2506.17612*, 2025. 2

[27] Shilong Liu, Zhaoyang Zeng, Tianhe Ren, Feng Li, Hao Zhang, Jie Yang, Qing Jiang, Chunyuan Li, Jianwei Yang, Hang Su, et al. Grounding dino: Marrying dino with grounded pre-training for open-set object detection. In *European conference on computer vision*, pages 38–55. Springer, 2024. 3, 2

[28] Shiyu Liu, Yucheng Han, Peng Xing, Fukun Yin, Rui Wang, Wei Cheng, Jiaqi Liao, Yingming Wang, Honghao Fu, Chunrui Han, et al. Step1x-edit: A practical framework for general image editing. *arXiv preprint arXiv:2504.17761*, 2025. 1, 2, 3, 6, 5, 9

[29] Chaojie Mao, Jingfeng Zhang, Yulin Pan, Zeyinzi Jiang, Zhen Han, Yu Liu, and Jingren Zhou. Ace++: Instruction-based image creation and editing via context-aware content filling. *arXiv preprint arXiv:2501.02487*, 2025. 2

[30] Aaron van den Oord, Yazhe Li, and Oriol Vinyals. Representation learning with contrastive predictive coding. *arXiv preprint arXiv:1807.03748*, 2018. 5

[31] Wenqi Ouyang, Yi Dong, Xiaoyang Kang, Peiran Ren, Xin Xu, and Xuansong Xie. Rsfnet: A white-box image retouching approach using region-specific color filters. In *Proceedings of the IEEE/CVF International Conference on Computer Vision*, pages 12160–12169, 2023. 2, 3, 6, 4, 5

[32] Alec Radford, Jong Wook Kim, Chris Hallacy, Aditya Ramesh, Gabriel Goh, Sandhini Agarwal, Girish Sastry, Amanda Askell, Pamela Mishkin, Jack Clark, et al. Learning transferable visual models from natural language supervision. In *International conference on machine learning*, pages 8748–8763. PMLR, 2021. 2

[33] Nikhila Ravi, Valentin Gabeur, Yuan-Ting Hu, Ronghang Hu, Chaitanya Ryali, Tengyu Ma, Haitham Khedr, Roman Rädle, Chloe Rolland, Laura Gustafson, et al. Sam 2: Segment anything in images and videos. *arXiv preprint arXiv:2408.00714*, 2024. 3, 2

[34] Robin Rombach, Andreas Blattmann, Dominik Lorenz, Patrick Esser, and Björn Ommer. High-resolution image synthesis with latent diffusion models. In *Proceedings of the IEEE/CVF conference on computer vision and pattern recognition*, pages 10684–10695, 2022. 2, 3

[35] Mehul P Sampat, Zhou Wang, Shalini Gupta, Alan Conrad Bovik, and Mia K Markey. Complex wavelet structural similarity: A new image similarity index. *IEEE transactions on image processing*, 18(11):2385–2401, 2009. 6, 9

[36] Florian Schroff, Dmitry Kalenichenko, and James Philbin. Facenet: A unified embedding for face recognition and clustering. In *Proceedings of the IEEE conference on computer vision and pattern recognition*, pages 815–823, 2015. 7

[37] Christoph Schuhmann and Romain Beaumont. Laion-aesthetics. *LAION. AI*, 2022. 3

[38] Shelly Sheynin, Adam Polyak, Uriel Singer, Yuval Kirstain, Amit Zohar, Oron Ashual, Devi Parikh, and Yaniv Taigman. Emu edit: Precise image editing via recognition and generation tasks. In *Proceedings of the IEEE/CVF Conference on Computer Vision and Pattern Recognition*, pages 8871–8879, 2024. 2

[39] Ethan Tseng, Yuxuan Zhang, Lars Jebe, Xuaner Zhang, Zhihao Xia, Yifei Fan, Felix Heide, and Jiawen Chen. Neural photo-finishing. *ACM Transactions on Graphics*, 41(6): 3555526, 2022. 3

[40] Peng Wang, Yichun Shi, Xiaochen Lian, Zhonghua Zhai, Xin Xia, Xuefeng Xiao, Weilin Huang, and Jianchao Yang. Seededit 3.0: Fast and high-quality generative image editing. *arXiv preprint arXiv:2506.05083*, 2025. 3

[41] Zhou Wang, Alan C Bovik, Hamid R Sheikh, and Eero P Simoncelli. Image quality assessment: from error visibility to structural similarity. *IEEE transactions on image processing*, 13(4):600–612, 2004. 6, 9

[42] Zhengyi Wang, Cheng Lu, Yikai Wang, Fan Bao, Chongxuan Li, Hang Su, and Jun Zhu. Prolificdreamer: High-fidelity and diverse text-to-3d generation with variational score distillation. *Advances in neural information processing systems*, 36: 8406–8441, 2023. 2

[43] Chenfei Wu, Jiahao Li, Jingren Zhou, Junyang Lin, Kaiyuan Gao, Kun Yan, Sheng-ming Yin, Shuai Bai, Xiao Xu, Yilei Chen, et al. Qwen-image technical report. *arXiv preprint arXiv:2508.02324*, 2025. 1, 2, 6, 5

[44] Jiarui Wu, Yujin Wang, Lingen Li, Fan Zhang, and Tianfan Xue. Goal conditioned reinforcement learning for photo finishing tuning. In *Advances in Neural Information Processing Systems*, pages 46294–46318. Curran Associates, Inc., 2024. 3

[45] Rongyuan Wu, Lingchen Sun, Zhiyuan Ma, and Lei Zhang. One-step effective diffusion network for real-world image super-resolution. *Advances in Neural Information Processing Systems*, 37:92529–92553, 2024. 4, 5

[46] Wufeng Xue, Lei Zhang, Xuanqin Mou, and Alan C Bovik. Gradient magnitude similarity deviation: A highly efficient perceptual image quality index. *IEEE transactions on image processing*, 23(2):684–695, 2013. 6, 9

[47] Tianwei Yin, Michaël Gharbi, Richard Zhang, Eli Shechtman, Fredo Durand, William T Freeman, and Taesung Park. One-step diffusion with distribution matching distillation. In *Proceedings of the IEEE/CVF conference on computer vision and pattern recognition*, pages 6613–6623, 2024. 2, 4, 5

[48] Hui Zeng, Jianrui Cai, Lida Li, Zisheng Cao, and Lei Zhang. Learning image-adaptive 3d lookup tables for high performance photo enhancement in real-time. *IEEE Transactions on Pattern Analysis and Machine Intelligence*, 44(4):2058–2073, 2020. 2, 3, 6, 4, 5

[49] Hong Zhang, Zhongjie Duan, Xingjun Wang, Yuze Zhao, Weiyi Lu, Zhipeng Di, Yixuan Xu, Yingda Chen, and Yu Zhang. Nexus-gen: A unified model for image understanding, generation, and editing. *arXiv preprint arXiv:2504.21356*, 2025. 3

[50] Kai Zhang, Lingbo Mo, Wenhu Chen, Huan Sun, and Yu Su. Magicbrush: A manually annotated dataset for instruction-guided image editing. *Advances in Neural Information Processing Systems*, 36:31428–31449, 2023. 2, 6, 9

[51] Zechuan Zhang, Ji Xie, Yu Lu, Zongxin Yang, and Yi Yang. In-context edit: Enabling instructional image editing with in-context generation in large scale diffusion transformer. *arXiv preprint arXiv:2504.20690*, 2025. 2

[52] Haozhe Zhao, Xiaojian Shawn Ma, Liang Chen, Shuzheng Si, Rujie Wu, Kaikai An, Peiyu Yu, Minjia Zhang, Qing Li, and Baobao Chang. Ultraedit: Instruction-based fine-grained image editing at scale. *Advances in Neural Information Processing Systems*, 37:3058–3093, 2024. 2

InstantRetouch: Efficient and High-Fidelity Instruction-Guided Image Retouching with Bilateral Space

Supplementary Material

Our supplementary material is organized as follows:

- **Sec. A: Datasets.** We provide more details of our proposed *iRetouch benchmark*, and explain the construction of our *training dataset*.
- **Sec. B: Fine-grained Regional Control.** We introduce an extension to our framework that enables *fine-grained regional control* over edits by leveraging bilateral grid blending.
- **Sec. C: Additional Experimental Results.** We present additional results, including evaluation on the *MIT-Adobe FiveK* dataset, expanded comparisons with more baselines and metrics on iRetouch, and additional ablation studies.
- **Sec. D: Additional Method Details.** We offer further details on our method.
- **Sec. E: Additional Experimental Details.** We outline key experimental specifics, including details of our *evaluation metrics*, a full breakdown of our *implementation*, and our *user study*.

A. Datasets

In this section, we provide a more detailed account of the construction process for both our **iRetouch benchmark** used for evaluation and the large-scale **training dataset** used to train our model.

A.1. iRetouch Benchmark

The iRetouch benchmark is designed to provide a comprehensive and realistic testbed for instruction-guided image retouching. It consists of 500 high-resolution before–and–after image pairs, accompanied by manually refined natural language instructions. The image pairs were curated from the Adobe Lightroom community, where professional photographers share their original and edited photos. We selected this source because it represents real-world editing scenarios, high-quality artistic intent, and a wide variety of photographic genres. The selected pairs cover a broad range of subjects, including portraits, landscapes, animals, still-life, macro/close-up, and street scenes, ensuring our benchmark is not biased towards a specific domain.

For each before–and–after pair, we first generated a candidate instruction using the same procedure as our training data generation (detailed in Sec. A.2), prompting a powerful Multimodal Large Language Model (MLLM) to describe the transformation. This was followed by a manual refinement process to ensure clarity, accuracy, and naturalness.

As shown in Fig. 8, our retouching instruction covers global adjustments (brightness up/down, contrast soft/hard, temperature warm/cool/neutral, saturation up/down/local), styles (cinematic, dreamy, vintage, black-and-white, high-/low-key), moods (cheerful, cozy, serene, moody, dramatic, nostalgic, ethereal), time and season (sunset/golden hour, night, astrophotography, autumn/spring/winter), locality (global edits, subject boosting, background darkening/softening, sky/water), subjects (landscape, city, animal, bird, macro, portrait, food, astro), targeted HSL channels (green, blue, yellow, orange, magenta), and effects/intensity (glow, fog, vignette, grain; subtle/strong). Crucially, it also includes instructions for local edits (e.g., subject boosting, background darkening/softening, sky/water enhancements). This diversity allows for a more accurate and comprehensive evaluation of instruction-guided image retouching methods.

A.2. Construction of Training Dataset

Our training dataset, comprising approximately 200K triplets of $(x, x^\star, c_T)$, was constructed via a three-stage pipeline. We first curated high-quality targets $x^\star$, then synthesized degraded inputs x, and finally generated corresponding instructions c_T. While the main paper provides an overview, here we detail the latter two stages.

Synthesis of Degraded Inputs (x). For each target $x^\star$, we generated a degraded input x by applying a randomized photo-finishing pipeline. This "inverse editing" process includes the following stochastic photometric adjustments:

- **Exposure:** Adjusts the overall image brightness by simulating more or less light capture during exposure.
- **Gamma:** Modifies mid-tone brightness without affecting the black and white points.
- **White Balance:** Corrects color casts by adjusting temperature (cool/blue to warm/yellow) and tint (green to magenta).
- **Contrast:** Alters the tonal range by making darks darker and lights lighter.
- **Tone Curves:** Provides fine-grained control over brightness across different tonal ranges via S-shaped curves.
- **Saturation:** Controls the intensity and vividness of all colors in the image.
- **Shadows/Highlights:** Recovers detail by specifically brightening dark areas (shadows) or darkening bright areas (highlights).
- **HSL:** Selectively adjusts the hue, saturation, or brightness of each primary color range.

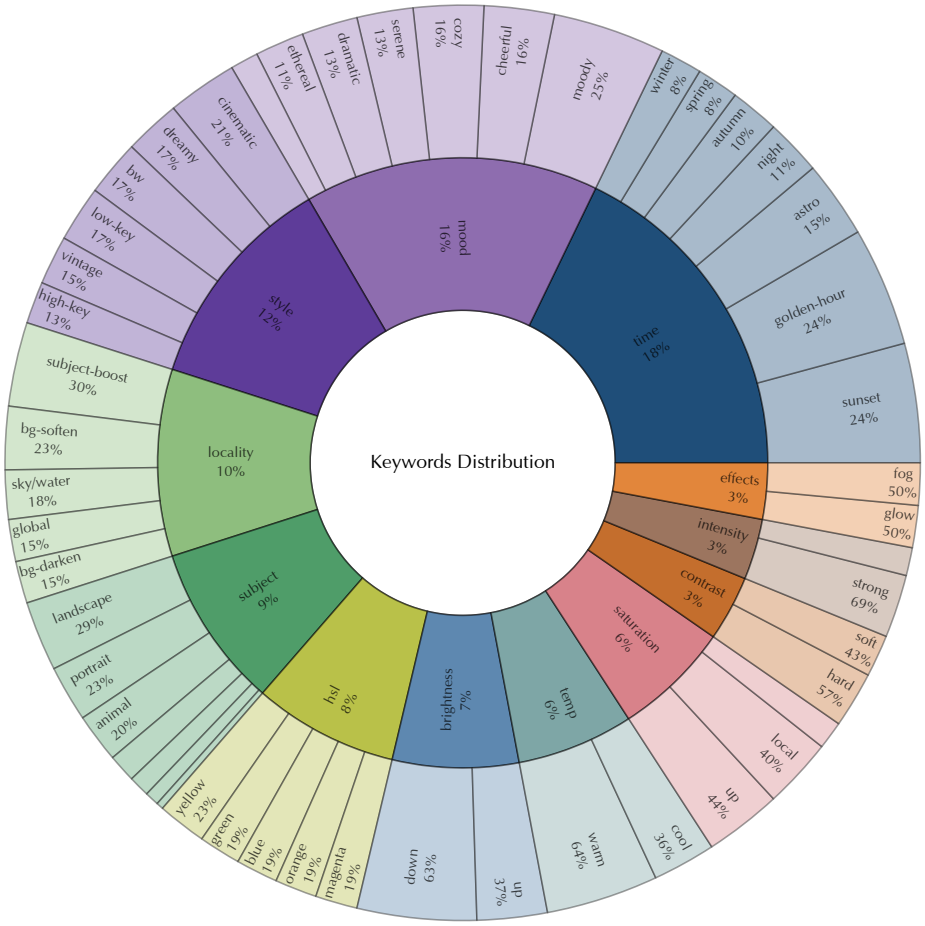

Figure 8. **Hierarchical keyword distribution of our iRetouch benchmark.** The sunburst chart illustrates the diversity and composition of the 500 instructions in our test set, spanning multiple semantic levels from high-level mood and style to specific adjustments like HSL channels and locality. This diversity ensures a comprehensive evaluation of instruction-guided retouching capabilities.

To prevent a bias towards extreme adjustments and to better model subtle, realistic edits, parameters for key operations like exposure were sampled from a Gaussian distribution centered on the no-op value (i.e., a mean of zero for additive adjustments). This ensures that a majority of our training examples represent moderate and fine-grained retouching, improving the model's generalization to real-world user requests.

For local adjustments, we generated masks from multiple sources. We used a Grounding-SAM procedure [27, 33] for semantic masks (e.g., "face", "sky"). To complement these, we also generated non-semantic, geometric masks from superpixel segmentations and simple priors like vertical/horizontal gradients. Applying different degradation parameters to this diverse set of masks allowed us to synthesize a rich variety of spatially varying edits.

Generation of Instructions (c_T). With an image pair $(x, x^\star)$ prepared, we prompted the Qwen2.5-VL-72B MLLM [1] to generate the corresponding instruction c_T. The prompt, shown in Fig. 16, was carefully engineered to elicit high-quality, user-centric instructions. Specifically, it instructs the model to adopt the persona of an "intuitive photo editing assistant" and to focus on the editing *intention* rather than the technical *action*. By providing rules and examples, the prompt steers the MLLM to produce concise, casual, and actionable instructions (e.g., "give it a warm sunset vibe") while strictly avoiding technical jargon (e.g., "increase temperature"). This approach was crucial for creating a training dataset that reflects how users naturally communicate their desired aesthetic goals.

B. Fine-grained Regional Control

Our model architecture naturally supports fine-grained regional control by blending transformations directly in the bilateral grid space. This allows for complex, fine-grained

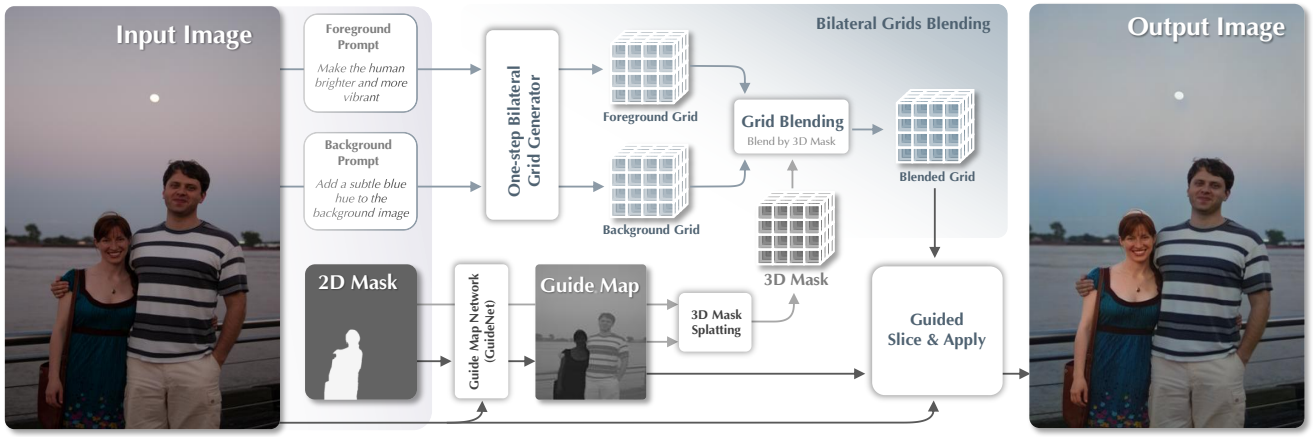

Figure 9. **An overview of our framework for fine-grained regional control.** Given an input image, a 2D mask, and distinct prompts for foreground and background, our model generates two separate bilateral grids ($\Gamma^{\text{fg}}, \Gamma^{\text{bg}}$). In parallel, a guide network produces a mask-aware guide map (z). The crucial step is lifting the 2D pixel mask (M_{pxl}) to a 3D grid mask (M_{grid}) via our proposed **3D Mask Splatting** procedure, using z for depth guidance. This enables a principled blend of the grids in coefficient space, producing a single fused grid (Γ^{fused}) that is rendered in one pass to create the final, artifact-free output.

Figure 10. **Qualitative results of fine-grained regional control through bilateral grid blending.** For each example, a user provides an input image, a 2D mask, and separate text prompts for the foreground and background. Our method successfully applies distinct and often complex edits to the specified regions. Note the seamless transitions at the mask boundaries and the high fidelity of the results, demonstrating the effectiveness of blending in the grid space.

localized edits, such as making one person brighter and keeping the other person in the dark (Fig. 10), while maintaining high visual quality and content fidelity. The core of this capability lies in our grid blending framework, which we detail below.

B.1. Framework for bilateral grids blending

Given a user-provided 2D mask $M_{\text{pxl}} \in \mathbb{R}^{H\times W\times 1}$ (which can be obtained from off-the-shelf models like SAM [33]) and distinct text prompts for the foreground and background regions, our goal is to produce a single, seamlessly edited image.

A naive solution would be to generate two separate images and alpha-blend them. However, this is inefficient as it requires two full-resolution rendering passes and often produces undesirable halo artifacts along the mask boundaries, especially when the two editing styles are significantly different.

We devise a more principled solution, outlined in Fig. 9, that interchanges the blending and rendering steps. First,

Algorithm 1 3D Mask Splatting

Require: Pixel mask M_{pxl}, guide map z, grid size (W_g, H_g, D), prior strength $\alpha \geq 0$, stabilizer $\varepsilon > 0$
Ensure: Grid mask M_{grid}

$N, C \leftarrow \text{zeros}(D, H_g, W_g)$ ▷ Value and weight accumulators
for each pixel (x, y) **do**
  $u \leftarrow x \cdot (W_g - 1)/(W - 1)$
  $v \leftarrow y \cdot (H_g - 1)/(H - 1)$
  $r \leftarrow z[y, x] \cdot (D - 1)$
  ▷ Map to continuous grid coordinate
  $\mathcal{S} \leftarrow \text{GetTriLinNeighborsAndWeights}(u, v, r)$
  ▷ Splat mask value to 8 tri-linear neighbors
  for each neighbor (d, h, w) with weight w_i in $\mathcal{S}$ **do**
    $N[d, h, w] \mathrel{+}= w_i \cdot M_{\text{pxl}}[y, x]$
    $C[d, h, w] \mathrel{+}= w_i$
  end for
end for
$M_{\text{grid}} \leftarrow \text{clip}\left(N/(C + \varepsilon), 0, 1\right)$
return M_{grid}

our model generates two distinct bilateral grids: a foreground grid $\Gamma^{\text{fg}} \in \mathbb{R}^{H_g \times W_g \times D}$ and a background grid $\Gamma^{\text{bg}} \in \mathbb{R}^{H_g \times W_g \times D}$, each corresponding to its respective prompt. In parallel, a lightweight guide network, conditioned on both the input image and the 2D mask, predicts a single, mask-aware guide map $z \in \mathbb{R}^{H \times W \times 1}$. The key challenge is then to blend Γ^{fg} and Γ^{bg} using the 2D mask M_{pxl}. To this end, we introduce a **3D Mask Splatting** procedure that lifts the 2D pixel mask $M_{\text{pxl}} \in \mathbb{R}^{H \times W \times 1}$ into a 3D grid mask $M_{\text{grid}} \in \mathbb{R}^{H_g \times W_g \times D}$, which can then be used to blend the grids directly.

B.2. 3D Mask Splatting and Grid-Level Blending

The splatting operation is the opposite of the standard bilateral grid "slicing." It ensures that the transformation respects the bilateral space structure and perfectly preserves constant-value regions.

The process, detailed in Algorithm 1, begins by mapping each pixel's 2D coordinate (x, y) and its corresponding guide value $z(x, y)$ to a continuous 3D coordinate within the grid. Instead of reading a value (as in slicing), we "splat" or distribute the pixel's mask value, $M_{\text{pxl}}(x, y)$, to the D integer grid cells surrounding the continuous coordinate, weighted by tri-linear interpolation coefficients. These weighted values are accumulated in a numerator grid N, while the weights themselves are summed into a denominator grid C. M_{grid} is then the stabilized ratio of N and C.

With the 3D grid mask constructed, we linearly blend the foreground and background coefficient grids:

$$\Gamma^{\text{fused}} = M_{\text{grid}} \odot \Gamma^{\text{fg}} + (1 - M_{\text{grid}}) \odot \Gamma^{\text{bg}}, \tag{11}$$

where $\odot$ is element-wise multiplication. The resulting Γ^{fused} is then used with the guide map z to render the final output in a single, efficient pass.

B.3. Training Objectives for Regional Control

To train the guide network and ensure mask fidelity, we introduce two additional loss terms.

Mask Fidelity Loss. To ensure the grid mask accurately represents the original 2D mask after slicing, we enforce a reconstruction loss. We slice the predicted 3D grid mask M_{grid} using the learned guide map z and penalize its L2 distance to the input pixel mask M_{pxl}:

$$\mathcal{L}_{\text{mask}} = \|\text{slice}(M_{\text{grid}}, z) - M_{\text{pxl}}\|_2^2. \tag{12}$$

This encourages the entire 3D mask generation pipeline to be self-consistent.

Guide Map Regularization. To prevent the guide network from producing arbitrary guide maps that might degrade slicing quality, we regularize the learned guide map z to stay close to the input image's luminance I_{gray}:

$$\mathcal{L}_{\text{guide}} = \|z - I_{\text{gray}}\|_2^2. \tag{13}$$

C. Additional Experimental Results

In this section, we provide more extensive quantitative and qualitative results to supplement the main paper. We first present a comprehensive comparison on our iRetouch benchmark, including more baselines, metrics, and additional visual comparison. We then report our performance on the standard MIT-Adobe FiveK dataset. We also perform additional ablation studies.

C.1. Additional Evaluation on iRetouch Benchmark

C.1.1. Additional Baselines and Metrics

To provide a more comprehensive comparison beyond the main paper, we present an expanded quantitative evaluation on our iRetouch benchmark in Tab. 4. This supplementary table introduces two key additions:

- **An additional baseline:** We include DiffRetouch [9], a recent state-of-the-art non-instructional image retouching algorithm, to further contextualize our performance among traditional methods.
- **Additional metrics:** We report scores from a suite of common No-Reference Image Quality Assessment (NR-IQA) models, namely MUSIQ [19], HyperIQA [54], and NIMA [55].

The results of these NR-IQA metrics reveal an important discrepancy: while our method outperforms all non-instructional retouching baselines [9, 31, 48] on these scores, it is surpassed by several large generative models,

Table 4. **Comprehensive comparison on our iRetouch benchmark.** We evaluate methods across four axes: efficiency, content fidelity, editing quality, and no-reference image quality (NR-IQA). Our method demonstrates superior content fidelity and efficiency while maintaining competitive editing and image quality, striking an optimal balance for the retouching task.

Method	Efficiency	Content Fidelity				Editing Quality					Image Quality		
	runtime↓	SSIM↑	CW-SSIM↑	GSMD↓	DISTS↓	L1↓	L2↓	SC↑	PQ↑	O↑	MUSIQ↑	HyperIQA↑	NIMA↑
3DLUT [48]	0.066	0.982	**0.981**	0.013	0.024	0.136	0.034	-	-	-	59.56	0.47	5.60
RSFNet [31]	0.029	0.975	0.976	**0.012**	0.038	0.137	0.034	-	-	-	58.29	0.43	5.58
DiffRetouch [9]	1.671	0.982	0.979	0.014	0.028	0.133	0.034	-	-	-	59.35	0.44	5.55
InstructPix2Pix [2]	4.632	0.742	0.768	0.149	0.177	0.164	0.050	7.11	7.58	7.34	48.00	0.33	5.48
Step1X-Edit [28]	57.932	0.706	0.694	0.174	0.167	0.140	0.036	7.63	8.52	8.06	67.22	0.50	5.90
GPT-Image-1 [17]	15.427	0.505	0.397	0.242	0.216	0.215	0.082	8.09	8.56	8.32	66.31	0.62	5.91
Qwen-Image [43]	7.720	0.689	0.744	0.174	0.147	0.168	0.054	8.12	8.67	8.39	63.57	0.52	5.78
FLUX.1-Kontext-Pro [22]	10.235	0.802	0.857	0.112	0.132	0.161	0.050	7.56	8.72	8.12	61.61	0.51	5.59
Gemini-2.5-Flash [6]	14.440	0.676	0.796	0.175	0.115	0.137	0.036	**8.56**	8.94	**8.74**	61.73	0.50	5.77
Ours	0.065	**0.989**	0.973	**0.012**	**0.022**	**0.099**	**0.018**	8.14	**8.98**	8.54	61.55	0.49	5.65

such as Step1X-Edit [28], GPT-Image-1 [17], and Qwen-Image [43]. This observation motivates a deeper investigation into the validity of NR-IQA metrics for the retouching task, as they appear to favor outputs that compromise content fidelity.

C.1.2. Discussion of NR-IQA Metrics for Retouching

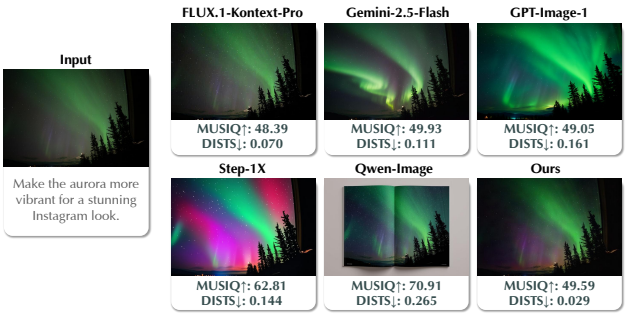

Figure 11. **Visual Case Study: NR-IQA (MUSIQ) vs. Content Fidelity (DISTS).** For the instruction to enhance the aurora, generative models achieve high MUSIQ scores by fabricating content (*e.g.*, Step-1X adds unnatural colors, Qwen-Image hallucinates a magazine). Our method faithfully enhances the scene, resulting in a slightly lower MUSIQ score but drastically better fidelity (low DISTS), which is the desired behavior for retouching.

Our analysis reveals a critical pitfall in using standard NR-IQA metrics for evaluating image retouching: generative models can "hack" these scores by sacrificing content fidelity. This phenomenon is illustrated by the visual case study in Fig. 11.

Given the instruction to make the aurora "more vibrant for a stunning Instagram look," generative models like Step-1X and Qwen-Image achieve remarkably high MUSIQ scores (62.81 and an astonishing 70.91, respectively). However, this comes at a devastating cost to fidelity, as reflected in their extremely poor DISTS scores (0.144 and 0.265). The visual results expose the reason for this discrepancy. Step-1X invents unrealistic, oversaturated magenta hues not present in the original scene. Moreover, Qwen-Image completely misinterprets the context and hallucinates the image into a magazine layout, yielding a numerically impressive but contextually meaningless MUSIQ score. Other models like GPT-Image-1 and Gemini-2.5-Flash significantly distort the natural shape and flow of the aurora.

In contrast, our method achieves a reasonable MUSIQ score (49.59) while maintaining exceptional fidelity (DISTS of just 0.029). Visually, our result successfully enhances the vibrancy and color of the aurora as it existed in the input, fulfilling the user's intent without fabricating content. This case study provides evidence that a high NR-IQA score in the context of generative editing often signals content alteration rather than faithful retouching. It underscores that for image retouching, fidelity-aware metrics and human judgment remain more reliable indicators of true performance.

C.1.3. Additional Visual Comparison

Fig. 14 provides further full-page visual comparisons across a diverse set of examples from our iRetouch benchmark. These results demonstrate our model's versatility in handling a wide range of scenarios. Across all examples, our method consistently produces high-quality, faithful edits that respect the original image content, unlike generative baselines that often introduce unintended content drifts.

C.2. Evaluation on MIT-Adobe FiveK Dataset

We further validate our method on the widely-used MIT-Adobe FiveK dataset [53], which contains 5,000 images, each retouched by five different experts (Experts A-E). For our evaluation, we use the 500-image test split and treat the edit by Expert C as the ground truth. Since this dataset lacks textual instructions, we use our instruction generation pipeline (detailed in Sec. A.2) to automatically create an instruction for each input-target pair.

Table 5. **Quantitative comparison on the MIT-Adobe FiveK dataset.** Our method significantly outperforms all baselines in content fidelity and achieves state-of-the-art editing quality, demonstrating its effectiveness on this standard benchmark.

Method	Content Fidelity				Editing Quality				
	SSIM↑	CW-SSIM↑	GSMD↓	DISTS↓	L1↓	L2↓	SC↑	PQ↑	O↑
InstructPix2Pix [2]	0.749	0.734	0.156	0.184	0.149	0.042	7.20	7.85	7.52
Step1X-Edit [28]	0.725	0.694	0.174	0.158	0.143	0.039	8.16	8.30	8.23
GPT-Image-1 [17]	0.543	0.452	0.229	0.219	0.212	0.083	**8.17**	8.60	8.38
Qwen-Image [43]	0.682	0.795	0.174	0.112	0.156	0.050	7.49	8.85	8.14
FLUX.1-Kontext-Pro [22]	0.791	0.733	0.123	0.111	0.159	0.051	7.28	8.91	8.05
Gemini-2.5-Flash [6]	0.641	0.762	0.183	0.106	0.154	0.047	7.72	8.98	8.33
Ours	**0.987**	**0.971**	**0.015**	**0.020**	**0.077**	**0.010**	7.87	**9.01**	**8.42**

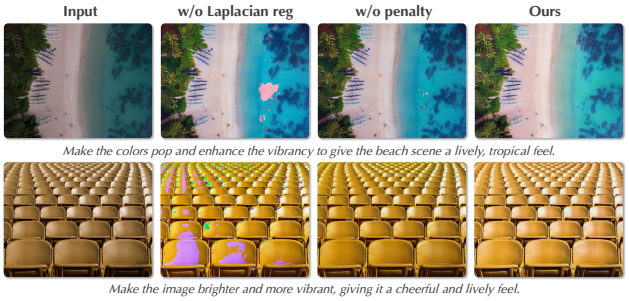

Figure 12. **Ablation study on the bilateral loss regularizers.** Removing the Laplacian regularizer introduces splotchy, spatially inconsistent artifacts. Removing the overflow penalty leads to severe color clipping and out-of-gamut colors. Our full method with both terms produces clean and high-quality results.

C.2.1. Quantitative Comparison

As shown in Tab. 5, our method again demonstrates dominant performance. It achieves the best scores across all four content fidelity metrics by a significant margin, confirming its exceptional ability to preserve image structure and details. Furthermore, it obtains the highest scores in editing quality metrics PQ and O, and a highly competitive SC score, indicating that the edits are both aesthetically pleasing and closely aligned with the expert's intent. The low L1 and L2 scores further underscore the precision of our edits.

C.2.2. Visual Comparison

The qualitative results on MIT-FiveK, shown in Fig. 15, further highlight the superiority of our approach in delivering high-fidelity, high-quality, and accurate retouching results.

C.3. Additional Ablation Studies

To validate the design choices of our bilateral loss function, $\mathcal{L}_{\text{bila}}$ (defined in Section 3.4.4 of the main paper), we conduct an ablation study on its key regularization components. Specifically, we analyze the effects of the 3D Laplacian regularizer on the bilateral grid ($\|\Delta^3\Gamma\|_2^2$) and the RGB overflow penalty ($\Psi(\hat{x}_B)$).

As visualized in Fig. 12, both components are crucial for generating clean, artifact-free results.

- **Without the Laplacian regularizer**, the model produces severe spatial artifacts. This demonstrates that the regularizer is essential for ensuring smoothness and spatial consistency in the predicted affine transformations.
- **Without the overflow penalty**, the edits suffer from harsh color clipping. Both examples exhibit large areas of blown-out highlights and unnatural color patches. This shows the penalty's effectiveness in preventing out-of-gamut colors and maintaining a natural, photographic appearance.

Our full method, which includes both terms, produces visually pleasing results that are smooth, vibrant, and free from these distracting artifacts, confirming the necessity of our proposed bilateral loss formulation.

D. Additional Method Details

D.1. Bilateral Space

Our full-resolution bilateral processing branch is central to achieving high-fidelity, efficient editing, particularly at high resolutions. Its design is rooted in the concept of the bilateral space, which we detail here to provide further context for our methodological choices.

The concept of bilateral space was first introduced by Paris and Durand [56] for fast, edge-aware image filtering. The core idea is to lift a 2D image $I(x, y)$ into a higher-dimensional space that jointly considers spatial and range (intensity) coordinates. In this augmented space, Euclidean distances naturally correspond to perceptual similarity, making operations inherently edge-aware. This process was made highly efficient via the *bilateral grid*, which reformulates the operation into three steps: **splatting** the input image's pixels onto a coarse, regular grid; **convolving** this low-resolution grid; and **slicing** the output by trilinearly interpolating from the grid at the original pixel coordinates. Since the computationally expensive convolution is performed on a small, fixed-size grid, the algorithm's runtime is effectively decoupled from the image resolution.

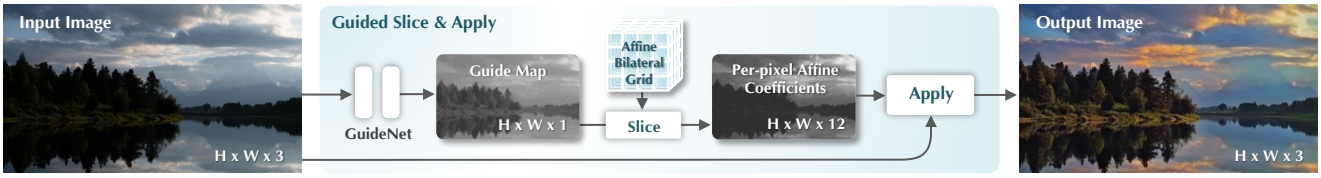

Figure 13. **An overview of our Guided Slice & Apply module.** This fully differentiable module operates at full resolution. First, a lightweight Guide Net processes the input image to produce a single-channel guide map. This map, along with the affine bilateral grid predicted by our adapter, is fed into the *Slice* operation. This operation performs a lookup to generate per-pixel affine coefficients. Finally, the *Apply* operation uses these coefficients to transform the original input pixels into the final retouched output, ensuring high-fidelity, edge-aware editing.

This framework was later extended from simple filtering to arbitrary image-to-image transformations by storing a locally affine model in each grid cell instead of a scalar value [5, 12]. Crucially, Gharbi et al. [12] demonstrated that the slicing operation is differentiable, which allows the bilateral grid to be integrated as a trainable layer in a deep neural network. In such a framework, a neural network learns to predict the parameters of the affine grid, which then transforms the input image to produce the final output. This formulation enforces strong priors on the output; as a locally affine transformation of the input, it is constrained from hallucinating novel textures or structures, thus preserving content fidelity and preventing common artifacts like amplified noise or false edges.

Our method builds upon this foundation by replacing the simple convolutional network used in prior work [12] with an instruction-guided one-step diffusion model. The role of our diffusion U-Net is not to render the final pixels, but to leverage its powerful semantic understanding to interpret the text prompt and input image, predicting the parameters of a single, low-dimensional affine bilateral grid. This predicted grid is then applied to the original, full-resolution input via the differentiable slicing operation. This design synergistically combines the strengths of both worlds: we harness the expressive power of generative models for complex, instruction-driven edits while inheriting the fundamental properties of the bilateral grid. This ensures our edits are high-fidelity, preserve subject identity, and remain exceptionally efficient across resolutions up to 4K, overcoming the key limitations of purely generative approaches.

D.2. Lightweight Bilateral Adapter

The Lightweight Bilateral Adapter is a convolutional network tasked with predicting the affine bilateral grid from the feature maps produced by our one-step diffusion branch. The architecture is designed to be efficient while effectively processing both local and global information.

The process begins by aligning the output features from the diffusion U-Net using a sequence of four convolutional layers. The resulting features are then passed to a stride-2 convolutional encoder to reduce spatial resolution. The network then splits into two parallel paths: (i) *Local Path:* This path consists of two stride-1 convolutional layers. By preserving the spatial resolution of its input features, this path focuses on capturing fine-grained local details necessary for spatially varying adjustments. (ii) *Global Path:* This path uses another stride-2 convolutional layer followed by three fully-connected layers to distill the features into a single global scene summary vector. This vector ensures the final transformation is spatially smooth and stable. The features from both paths are then fused. The global feature vector is broadcast and added to the local feature map at every spatial location. The fused feature map is then passed through a final linear layer to generate the affine bilateral grid, which has a shape of $B \times H_g \times W_g \times D \times 12$, where (H_g, W_g, D) are the dimensions of the coarse grid and 12 represents the parameters of a 3×4 affine matrix.

D.3. Guided Slice and Apply

As illustrated in Fig. 13, the Guided Slice & Apply module is a fully differentiable operation that applies the predicted edit to the full-resolution image. It takes the affine bilateral grid and the original input image, producing the final retouched output. The process can be broken down into three main steps:

Guide Map Generation. The full-resolution input image (size $H \times W \times 3$) is first passed through a lightweight Guide Net. This network consists of three convolutional layers and outputs a full-resolution, single-channel guide map (size $H \times W \times 1$). This map serves as the range (intensity) coordinate for the subsequent slicing operation.

A design choice here is the use of a *learned* Guide Net instead of a fixed function like a simple grayscale conversion. This is because different colors (RGB values) can map to the same intensity value. If such colors appear adjacent to each other at an important edge, a simple grayscale guide would map them to similar coordinates in the bilateral space. This would cause them to sample from the same or nearby cells in the bilateral grid, leading to a blurring of the edit across that edge. By learning the guide map, the

Table 6. The complete Attribute Bank for the $\mathcal{L}_{\text{align}}$ loss. The bank is organized into a two-part layout for readability. Each attribute provides a positive/negative prompt pair for stable, directional contrastive learning.

Part 1: Core Adjustments, Effects, & Styles			
Category	**Attribute**	**Positive Prompt**	**Negative Prompt**
Brightness	`up`	Bright Image	Dark Image
	`down`	Dark Image	Bright Image
Contrast	`up`	High Contrast Image	Low Contrast Image
	`down`	Low Contrast Image	High Contrast Image
	`hard`	High Contrast Image	Low Contrast Image
	`soft`	Low Contrast Image	High Contrast Image
Temperature	`warm`	Warm Color Temperature	Cool Color Temperature
	`cool`	Cool Color Temperature	Warm Color Temperature
	`neutral`	Neutral Color Temperature	Tinted Color Temperature
Saturation	`up`	High Saturation Image	Low Saturation Image
	`down`	Low Saturation Image	High Saturation Image
Vibrance	`up`	High Vibrance Colors	Muted Colors
	`down`	Muted Colors	High Vibrance Colors
Clarity	`up`	Sharp Detailed Image	Soft Blurry Image
	`down`	Soft Blurry Image	Sharp Detailed Image
Haze	`up`	Hazy Foggy Scene	Clear Dehazed Scene
	`down`	Clear Dehazed Scene	Hazy Foggy Scene
Effects	`glow_on`	Soft Glow Effect	No Glow Effect
	`fog_on`	Foggy Scene	Clear Air Scene
	`vignette_on`	Vignette Effect	No Vignette
	`grain_on`	Film Grain Effect	Clean Image
Style	`cinematic`	Cinematic Color Grading	Neutral Documentary Look
	`dreamy`	Dreamy Soft Look	Crisp Clinical Look
	`vintage`	Vintage Film Look	Modern Clean Look
	`bw`	Black and White Photo	Color Photo
	`high-key`	High-Key Lighting Photo	Low-Key Lighting Photo
	`low-key`	Low-Key Lighting Photo	High-Key Lighting Photo

Part 2: Moods, Time, HSL, & Intensity			
Category	**Attribute**	**Positive Prompt**	**Negative Prompt**
Mood	`cheerful`	Cheerful Color Grading	Gloomy Color Grading
	`cozy`	Cozy Warm Look	Cold Sterile Look
	`serene`	Serene Calm Look	Tense Dramatic Look
	`moody`	Moody Dark Look	Bright Cheerful Look
	`dramatic`	Dramatic Look	Flat Calm Look
	`nostalgic`	Nostalgic Look	Contemporary Clean Look
	`ethereal`	Ethereal Soft Look	Grounded Realistic Look
Time/Season	`sunset`	Sunset Colors	Neutral Daylight Colors
	`golden-hour`	Golden Hour Warm Light	Midday Neutral Light
	`night`	Nighttime Photo	Daytime Photo
	`astro`	Astrophotography Night Sky	Daylight Sky Photo
	`autumn`	Autumn Warm Foliage Colors	Neutral Foliage Colors
	`spring`	Spring Fresh Colors	Neutral Colors
	`winter`	Winter Cool Tones	Neutral Tones
HSL Adjust	`green:up`	More Green Tones	Less Green Tones
	`green:down`	Less Green Tones	More Green Tones
	`blue:up`	More Blue Tones	Less Blue Tones
	`blue:down`	Less Blue Tones	More Blue Tones
	`yellow:up`	More Yellow Tones	Less Yellow Tones
	`yellow:down`	Less Yellow Tones	More Yellow Tones
	`orange:up`	More Orange Tones	Less Orange Tones
	`orange:down`	Less Orange Tones	More Orange Tones
	`magenta:up`	More Magenta Tones	Less Magenta Tones
	`magenta:down`	Less Magenta Tones	More Magenta Tones
Intensity	`subtle`	Subtle Edit	Strong Edit
	`strong`	Strong Edit	Subtle Edit

network can create a representation that better separates distinct colors, thereby preserving sharp edges and enhancing the expressive power of the bilateral solution.

Slicing for Per-Pixel Coefficients. The *Slice* operation is the core of the bilateral framework. For each pixel at spatial coordinate (x, y) in the input image, we use its corresponding value from the guide map, $g(x, y)$, as the third coordinate. This forms a 3D coordinate $(x, y, g(x, y))$ which is used to look up a value from the low-resolution affine bilateral grid. This lookup is performed via fast tri-linear interpolation from the 8 neighboring cells in the grid. The result of this operation is a full-resolution tensor of per-pixel affine coefficients with shape $H \times W \times 12$. Each 12-dimensional vector corresponds to the interpolated affine transformation for that specific pixel.

Applying the Transformation. The final *Apply* step performs the color transformation. For each pixel, its 12 affine coefficients are reshaped into a 3×4 affine matrix. This matrix is then multiplied with the homogeneous coordinate vector of the corresponding pixel from the original input image, $[R, G, B, 1]^T$. This computes the new RGB values for the output pixel, effectively applying the locally varying, instruction-guided edit to produce the final, high-fidelity output image.

D.4. Details of Prompt Alignment Loss

In the main paper, we introduced the prompt alignment loss, $\mathcal{L}_{\text{align}}$, as a crucial component to ensure our one-step model accurately follows user instructions. Distilling a multi-step diffusion editor can weaken the coupling between the text prompt and the generated output, especially for compositional, directional edits common in photo retouching (e.g., "make it a bit warmer and cozier"). The $\mathcal{L}_{\text{align}}$ loss counteracts this by providing strong, explicit directional supervision. This section provides a detailed breakdown of the attribute matching pipeline and the complete attribute bank used to compute this loss.

The core idea is to convert a free-form user instruction c_T into a small, stable set of atomic retouching attributes $\mathcal{A}(c_T)$. Each attribute corresponds to a predefined positive/negative text prompt pair from our attribute bank (see Table 6). To robustly perform this mapping, we employ a multi-stage pipeline:

1. **Rule-Based Matching:** We first apply a fast, rule-based matcher that uses keyword and pattern matching to identify attributes. For example, an instruction containing "increase brightness" or "make it brighter" will be mapped to the `brightness:up` attribute. Similarly, "cinematic mood" maps to `style:cinematic`.
2. **Attribute Capping:** To ensure training stability and pre-

vent conflicting signals from overly complex prompts, we cap the number of matched attributes at a maximum of three. The three attributes with the highest confidence scores from the rule-based matcher are selected.

3. **LLM Fallback:** If the rule-based matcher fails to identify any attributes (i.e., $|\mathcal{A}(c_T)| = 0$), we employ a large language model (LLM) as a fallback mechanism. The LLM is prompted to perform the same task: analyze the instruction c_T and map it to one or more attributes from our predefined bank. This significantly increases the robustness of our matching process for unconventional or creative instructions. The prompt template is shown in Fig. 17.
4. **Loss Omission:** In the rare case that both the rule-based matcher and the LLM fallback fail to find any corresponding attributes, the prompt alignment loss term is simply omitted for that specific training instance.

Once the set of attributes $\mathcal{A}(c_T)$ is determined, the final loss is calculated as the average of the per-attribute InfoNCE losses, as defined in Eq. 6 of the main paper. This structured approach turns potentially weak or ambiguous instructions into strong, reliable supervision signals that guide the model toward the desired semantic direction.

E. Additional Experimental Details

E.1. Metrics Details and Justification

Content Fidelity Metrics. The core principle of image retouching is to enhance, not replace. An edit must preserve the original scene's structure and textures. To evaluate this rigorously while factoring out intentional, instruction-guided changes in color and tone, we perform a preprocessing step before calculating fidelity metrics. We first convert both the model's output and the ground truth to grayscale. Then, we apply histogram matching to the model's output, aligning its tonal distribution with that of the input image's grayscale version. This ensures our metrics focus purely on structural and textural integrity. On these processed images, we compute:

- **SSIM** [41]: Measures perceptual similarity based on structure, luminance, and contrast.
- **CW-SSIM** [35]: A complex wavelet variant of SSIM, more sensitive to geometric and textural distortions.
- **DISTS** [8]: A learned metric that explicitly models textural similarity and is highly correlated with human perception of distortion.
- **GMSD** [46]: Measures the deviation of gradient magnitudes, effectively capturing local structural changes.

Editing Quality Metrics. To assess how well the model follows instructions and the aesthetic quality of the result, we use several metrics. L1 and L2 distances are computed against the ground truth to measure pixel-level accuracy. Following recent work [28, 50], we also employ GPT-4o to provide automated ratings for:

- **SC (Score-Correctness, 0-10):** Instruction-image alignment.
- **PQ (Perceptual Quality, 0-10):** Overall perceptual quality.
- **O (Overall Score):** The geometric mean $\sqrt{\text{SC} \times \text{PQ}}$ to balance both aspects.

The prompt template used to elicit these scores from GPT-4o is detailed in Fig. 18.

Justification on No-Reference IQA (NR-IQA). In our experiments (Sec. C.1.2), we observed that generative models often achieve high NR-IQA scores (*e.g.*, MUSIQ, HyperIQA) at the cost of severely degraded content fidelity. These NR-IQA models, trained on diverse web data, tend to reward clear details, which generative models can "hack" by hallucinating new textures or altering content. For the task of retouching, where preserving the original subject matter is paramount, this behavior is undesirable. Therefore, while we report NR-IQA scores for completeness, we argue that fidelity-aware metrics (DISTS, SSIM) and reference-based quality metrics (L1/L2, SC/PQ) are more reliable indicators of true performance in the context of image retouching.

E.2. Additional Implementation Details

Our model is built upon a pre-trained InstrucPix2Pix model [2]. We initialize our U-Net weights from this pre-trained model and keep the VAE frozen throughout training. Our training process follows a two-stage progressive distillation strategy.

Stage 1: Low-Resolution Branch Distillation. In this stage, we exclusively train the low-resolution one-step diffusion branch (ϵ_θ) and its VSD regularizer ($\epsilon_{\phi'}$). Training in this stage follows a three-phase curriculum that anneals the VSD timestep t and adjusts loss weights, as detailed in Tab. 7. This curriculum strategy guides the model to first learn coarse structure (high t), then focus on instruction alignment (mid t), and finally refine subtle details (low t). The total loss for this stage is $\mathcal{L}_{\text{stage1}} = \mathcal{L}_{\text{data}} + \lambda_{\text{VSD}}\mathcal{L}_{\text{VSD}} + \lambda_{\text{align}}\mathcal{L}_{\text{align}}$.

Table 7. Three-phase curriculum for Stage 1 training.

VSD Timestep Range	Loss Function Composition	Training Steps
$[400, 800]$	$\mathcal{L}_{\text{vsd}} + 10 \cdot \mathcal{L}_{\text{data}}$	40k
$[200, 400]$	$\mathcal{L}_{\text{vsd}} + 2 \cdot \mathcal{L}_{\text{data}} + \mathcal{L}_{\text{align}}$	40k
$[50, 200]$	$\mathcal{L}_{\text{vsd}} + 0.5 \cdot \mathcal{L}_{\text{data}} + \mathcal{L}_{\text{align}}$	40k

Stage 2: Joint Bilateral Distillation. After Stage 1 converges (after 120k steps), we unfreeze the lightweight bilateral adapter and train the entire network end-to-end for an additional 80k steps. The loss function is augmented with our bilateral loss: $\mathcal{L}_{\text{stage2}} = \mathcal{L}_{\text{stage1}} + \lambda_{\text{bila}}\mathcal{L}_{\text{bila}}$. This stage fine-tunes the full pipeline, teaching the bilateral branch to generate high-fidelity, full-resolution edits.

Hyperparameters. We train our model at a 512x512 resolution with a total batch size of 64. We use the AdamW optimizer with a learning rate of 1×10^{-4}. We use automatic mixed-precision training for efficiency and apply gradient clipping with a max norm of 1.0. An exponential moving average (EMA) of the model weights is maintained with a decay rate of 0.999.

E.3. Additional User Study Details

To complement our quantitative analysis, we conducted a subjective user study to assess human preference.

Setup. The study involved 30 participants with diverse backgrounds. We drew 20 examples from our iRetouch benchmark for each user, covering a wide range of instructions. For each example, we presented the original image and the text instruction, followed by five edited results generated by our method and four leading baselines (FLUX.1-Kontext-pro, Gemini-2.5-Flash, Qwen-Image, GPT-Image-1).

Procedure. To ensure impartiality, the five results were displayed in a randomized order and labeled anonymously as 'A', 'B', 'C', 'D', and 'E'. Participants were unaware of which method corresponded to each label. For each example, they were asked to evaluate the five results based on four distinct criteria by answering the following questions:

- **Content Fidelity:** "Which result best enhances the image while preserving the original content and structure, without adding or removing objects/textures?"
- **Editing Ability:** "Which result most accurately and effectively follows the given text instruction?"
- **Visual Quality:** "Ignoring the instruction for a moment, which result has the highest overall visual and aesthetic quality (e.g., pleasing colors, no artifacts)?"
- **Overall Preference:** "If you had to choose only one edited image to keep or share, which one would you pick?"

Participants were asked to select the single best option for each question. The aggregated results, presented in Fig. 4 of the main paper, show a clear and consistent preference for our method across all four dimensions, validating its superior performance in producing high-fidelity, instruction-aligned, and aesthetically pleasing edits.

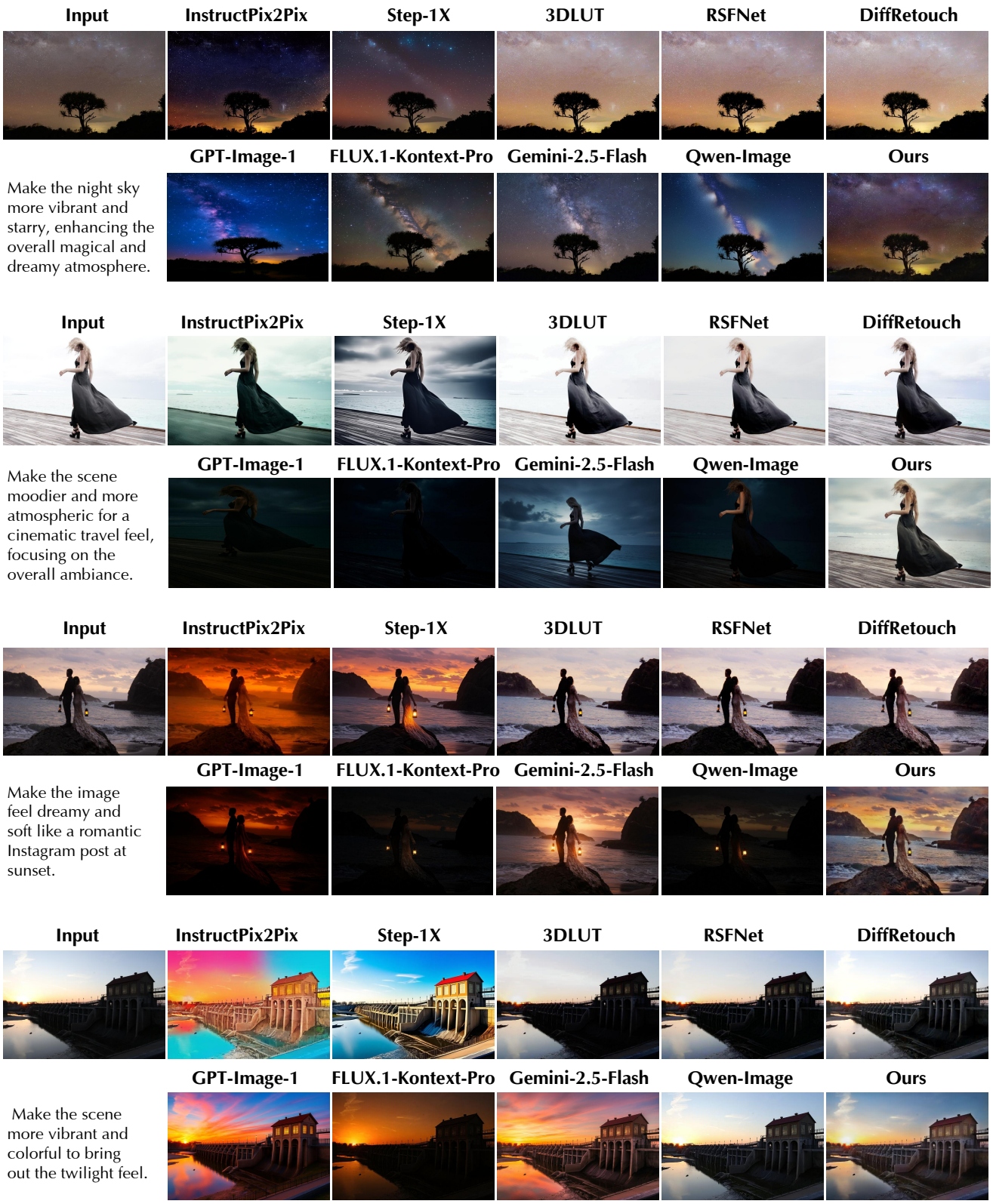

Figure 14. **Additional visual comparisons on our iRetouch benchmark.** Our method produces high-fidelity results that accurately follow the instructions, while baselines often alter content or fail to produce the desired effect.

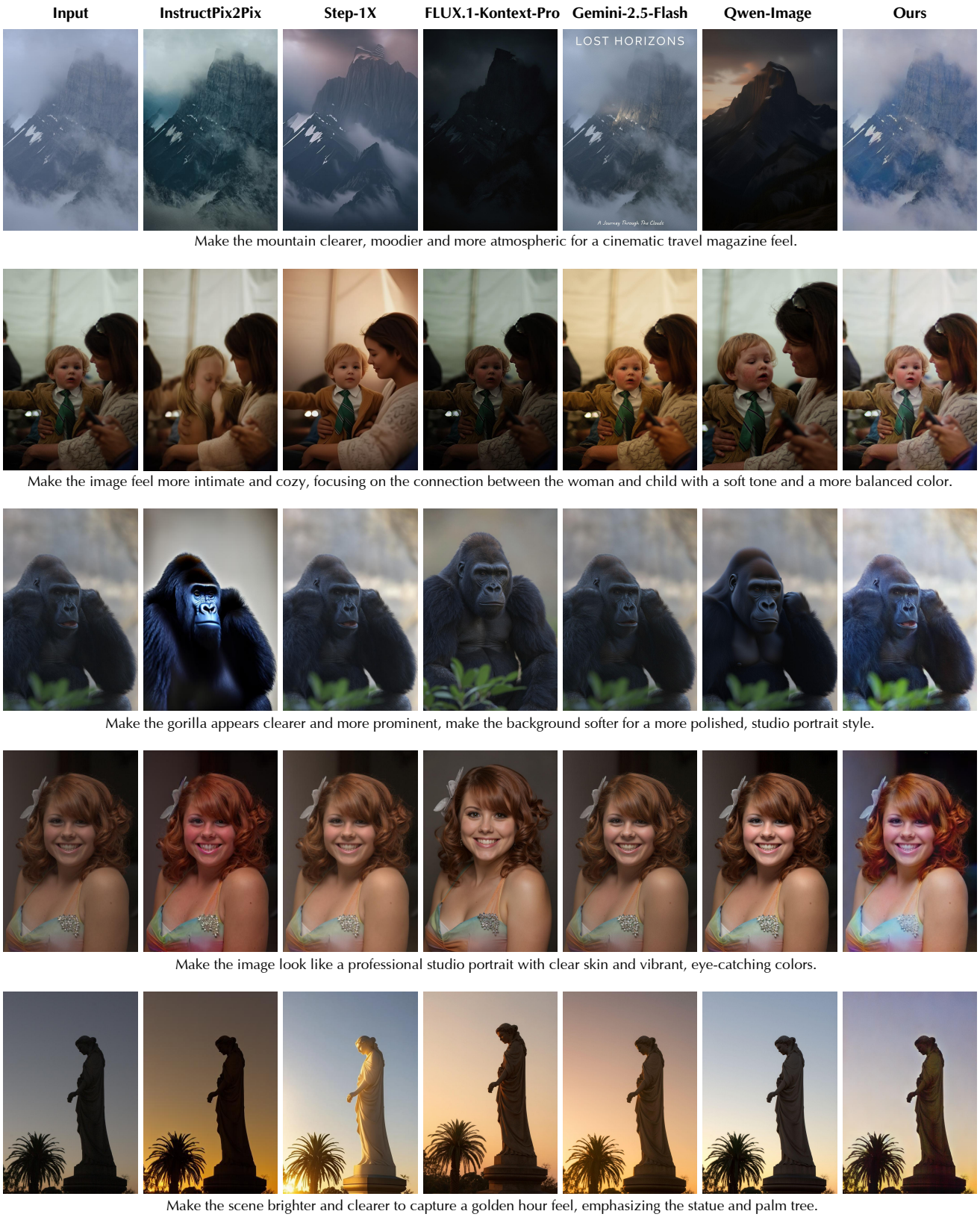

Figure 15. **Qualitative comparison on the MIT-Adobe FiveK dataset.** Our method demonstrates a superior ability to interpret complex, nuanced instructions and produce faithful, high-quality results compared to leading generative models, which often introduce unwanted repaints or hallucinate content.

Prompt Template for MLLM-based Instruction Generation

System Prompt

You are a helpful and intuitive photo editing assistant that interprets image edits from the perspective of an everyday user.

Your task is to analyze two images:

- The first is the original image before editing.
- The second is the edited version.

From these, infer the editing intention behind the changes, and express this intention as a natural, casual instruction that a general user might give to a photo editor.

User Prompt

Special Instructions:

1. Simulate a real person describing how they want the image to look — in casual, business-friendly English, not technical terms.
2. Describe the editing **intention** and **overall style** ("make it moodier", "give it a cinematic look", "add a warm sunset vibe", etc.), not the editing **action** ("increase contrast").
3. Do **not** describe what changed in the image. Instead, say what the user wanted to achieve with the edit.
4. Use **relatable terms** and style descriptors — e.g., "Instagram look", "studio portrait style", "vintage tone", "travel magazine feel", and more.
5. Avoid any numeric values or technical jargon (e.g., "exposure +1", "saturation 15").
6. Keep the instruction short — ideally one sentence under 20 words. **NO** quotation marks or special formatting.
7. If there were localized changes (e.g., face brightening, making certain area more prominent, etc.), include those intentions smoothly into the sentence. Look for enhancing specific features like making certain areas brighter, darker, more vibrant, or more prominent.

Examples (maybe some are too long, refer to the sentence structure only, ensure diversity of sentence structures):

1. Enhance the cat's eyes to pop more for a striking Instagram look while keeping the background soft and dreamy.
2. Make the sky brighter and warmer to enhance the sunset vibe and create a more vibrant, uplifting atmosphere.
3. I want this to look like it's straight out of a movie with depth, atmosphere, and film texture. Make the person clearer, smooth the skin, and enhance the jacket's colors and details.
4. Make my face look brighter and my eyes to stand out more. Can you make the skin smoother and the hair darker? Enhance the whole image without over-saturating colors.

Input:

Original Image: <img_1>
Edited Image: <img_2>

Output (Editing Intention):

Figure 16. **The complete prompt template used to guide the MLLM for instruction generation.** This structured prompt is designed to elicit user-centric, intention-focused descriptions of photo edits. By adopting a specific persona and following a set of detailed rules and examples, the model learns to generate concise and natural language instructions that form our training data.

Prompt Template for Instruction Parsing (LLM Fallback)

You are given multiple image editing instructions and an attribute OPTIONS dictionary.

For each instruction, pick ZERO, ONE, or MULTIPLE matching attributes (category+key) from OPTIONS. Also set `local_hint=true` if the instruction targets a region/object (e.g., sky, skin, grass, rose, background, subject); else `false`.

Return STRICT JSON with this schema:

```
{
  "results": [
    {"i": <int>, "matches": [{"category": <str>, "key": <str>, ...]},
    ...
  ]
}
```

Rules:

- Only use keys exactly from OPTIONS.
- If nothing fits, return `matches: []` for that item.
- Do NOT output extra text.

DATA:

```
{
  "instructions": [
    {
      "i": 0,
      "text": "make the sunset clouds more dramatic"
    },
    {
      "i": 1,
      "text": "give it a soft, dreamy feel"
    }
  ],
  "options": {
    "brightness": ["up", "down"],
    "contrast": ["up", "down", "hard", "soft"],
    "temp": ["warm", "cool", "neutral"],
    "saturation": ["up", "down"],
    "vibrance": ["up", "down"],
    "clarity": ["up", "down"],
    "haze": ["up", "down"],
    "effects": ["glow_on", "glow_off", "vignette_on", ...],
    "style": ["cinematic", "dreamy", "vintage", "bw", ...],
    "mood": ["cheerful", "cozy", "serene", "moody", ...],
    "time": ["sunset", "golden-hour", "night", "astro", ...],
    "hsl": ["green.up", "green.down", "blue.up", "blue.down", ...]
  }
}
```

Figure 17. **The prompt template for our LLM-based instruction parser.** This prompt provides the LLM with a list of user instructions and a dictionary of valid, predefined attributes. The model is tasked with returning a structured JSON object that maps each instruction to one or more corresponding edits from the dictionary, including a hint for whether the edit is local. This mechanism acts as a robust fallback, translating complex or ambiguous requests into pre-defined attributes.

Prompt Template for MLLM-based Evaluation

System Prompt

You are a post-production specialist with expertise in enhancing photographic imagery through advanced digital editing techniques. We now need your help to evaluate the performance of an AI-powered image post-editing tool for photography.

User Prompt

INPUTS:

1. Two images will be provided: The first being the original photographic image and the second being an edited version of the first.
2. The editing instruction will be provided: The post-editing needs of photographic images expressed by users with no image processing knowledge.

METRICS (From scale 0 to 10):

User Instruction Satisfaction Score: A score from 0 to 10 will be given based on how well the edits follow the user's instructions.

- Users typically have both global and local editing requirements when working with photographic images. Therefore, this score should be evaluated holistically, taking into account the user's needs for both local and global adjustments, with equal importance given to each.
- 0 indicates that the edited image does not follow the editing instruction at all.
- 10 indicates that the edited image follows the editing instruction text perfectly.

Perceptual Quality Score: A second score from 0 to 10 will rate the visual quality of the image after editing.

- Need to evaluate visual quality regarding image naturalness, artifacts and aesthetic quality.
- The edited image should look natural. It should have a natural color, lighting and photorealistic appearance.
- Need to compare before and after images to assess image artifacts. The edited image should prevent visual artifacts, such as content drifts, texture distortion, subjects not harmonized, etc.
- 0 indicates that the edited image does not look natural at all or contains a large portion of artifacts such as distortion, blurred faces, or subjects not harmonized.
- 10 indicates that the edited image looks natural and has no artifacts.

You will have to give your output in this way (Keep your reasoning concise and short.):

```
{
"score" : [score1, score2],
"reasoning" : "..."
}
```

Put the score in a list such that output score = [score1, score2], where 'score1' evaluates the User Instruction Satisfaction Score and 'score2' evaluates the Perceptual Quality Score.

Editing instruction:

Figure 18. **The complete prompt template for MLLM-based evaluation.** The MLLM, acting as a post-production specialist, assesses an AI-edited image based on two criteria: fidelity to the user's instruction and overall perceptual quality. It outputs a structured JSON with scores and a brief rationale.

References

[53] Vladimir Bychkovsky, Sylvain Paris, Eric Chan, and Frédo Durand. Learning photographic global tonal adjustment with a database of input/output image pairs. In *CVPR*, pages 804–811, 2011.

[54] Shaolin Su, Qingsen Yan, Yu Zhu, Cheng Zhang, Xin Ge, Jinqiu Sun, and Yanning Zhang. Blindly Assess Image Quality in the Wild Guided by a Self-Adaptive Hyper Network. In *IEEE/CVF Conference on Computer Vision and Pattern Recognition (CVPR)*, 2020.

[55] Hossein Talebi and Peyman Milanfar. NIMA: Neural Image Assessment. *IEEE Transactions on Image Processing*, 27(8):3998–4011, 2018.

[56] Sylvain Paris and Frédo Durand. A fast approximation of the bilateral filter using a signal processing approach. *International Journal of Computer Vision*, 81(1):24–52, 2009.